Research Article

Linus Yinn Leng Ang*, Fangsen Cui, Hee Joo Poh

Benchmarking the aircraft noise mapping package developed for a unified urban environmental modelling tool

https://doi.org/10.1515/noise-2024-0001 received January 26, 2024; accepted March 04, 2024

Abstract: In densely populated cities, residents living near aerodromes may experience heightened exposure to aircraft noise. With hybrid work arrangement, authorities have observed a rise in the number of complaints filed by residents affected by aircraft noise. In view of this problem, urban planners are now placing even more emphasis on exploring solutions that can manage aircraft noise in new and existing residential areas. To achieve this objective, urban planners usually rely on external acoustic consultants to generate noise maps using commercial software. However, urban planners may need to quickly evaluate potential noise issues in the neighbourhood so that noise management strategies can be brainstormed in advance. In this article, we present the development and benchmarking of a package designed to easily generate aircraft noise maps via simplified procedures and a reduced amount of input data, with acceptable accuracy in the results. These benefits distinguish our developed package from commercial software. Our developed package was eventually integrated into an in-housedeveloped unified urban environmental modelling tool that aims to help urban planners design more liveable and sustainable residential towns in an intuitive and quick manner.

Keywords: aircraft noise, urban noise, software development, environmental modelling, urban planning

1 Introduction

The recent emphasis on building sustainable and smart cities has driven advancements and innovative approaches related to noise mapping, a crucial domain within environmental acoustics [1-3]. While environmental noise encompasses a range of sources including road traffic, aircraft, and railways, research has predominantly concentrated on managing road traffic noise. Cutting-edge technologies such as advanced real-time evaluation techniques [4,5] and the application of artificial intelligence [6-8] have revolutionised noise mapping methodologies, allowing for more accurate and comprehensive assessments. Enhanced monitoring stations equipped with sophisticated sensors enable precise data collection, facilitating detailed analyses of noise distribution patterns and trends [9,10]. Recent attention has been directed towards electric vehicle transportation [11-13] and low-noise pavements [14,15], acknowledging their potential contributions to reducing overall urban noise pollution.

Many organisations have formally retained hybrid work arrangement to provide employees with flexibility [16]. For example, eligible employees are encouraged to work in the office for at least 3 days per week. For the remaining days, they are given the option to work remotely. Some organisations believe that remote work can help boost productivity among employees because less time is spent on getting ready and commuting [17]. In addition, formalising hybrid work arrangement can be seen as an opportunity for organisations to cut down on rental expenditures because less office space is needed. As more organisations formally include hybrid work arrangement in their policies, the stay-home population during office hours is expected to be large.

Following the ease of cross-border travel restrictions, air traffic is picking up to pre-pandemic levels. Although this improving situation is a good sign of economic recovery, the built environment is again polluted with aircraft noise like how it was before the pandemic. In the past, air traffic was already high, but employees rarely had the option to

^{*} Corresponding author: Linus Yinn Leng Ang, Institute of High Performance Computing (IHPC), Agency for Science, Technology and Research (A*STAR), 1 Fusionopolis Way, #16-16 Connexis, Singapore 138632, Republic of Singapore, e-mail: linus_ang@ihpc.a-star.edu.sg Fangsen Cui, Hee Joo Poh: Institute of High Performance Computing (IHPC), Agency for Science, Technology and Research (A*STAR), 1 Fusionopolis Way, #16-16 Connexis, Singapore 138632, Republic of Singapore

work remotely. With hybrid work arrangement, authorities have observed a rise in the number of complaints filed by residents due to aircraft noise. Despite the many modes of transport that contribute to noise pollution, research has shown that aircraft noise plays a significant role in determining how annoying the noise pollution is.

For example, Wothge et al. [18] surveyed more than 9,500 residents around Frankfurt Airport (Germany) in 2017 to study the influence of aircraft noise combined with another transportation noise - either railway or road traffic - on annoyance. The findings showed that residents would feel annoved whenever aircraft noise dominated the other transportation noise. In Switzerland, Schäffer et al. [19] surveyed more than 5,500 residents in 2020 to study the impact of green spaces on annoyance resulting from road traffic noise, railway noise, and aircraft noise. The survey found that with more green spaces, residents would feel less annoyed by railway noise and road traffic noise. However, for aircraft noise, residents continued to feel annoyed despite having more green spaces. In 2019, the World Health Organisation published the environmental noise guidelines for the European region [20], offering evidence-based conclusions that, at equivalent noise levels, aircraft noise induces greater annoyance compared to road traffic and railway noise.

Although aircraft noise is the leading contributor of annoyance among residents, evidence remains lacking in proving how chronic aircraft noise exposure can afflict mental health [21]. Nevertheless, research has firmly established that chronic exposure to aircraft noise can indirectly lead to health issues, such as cognitive impairment in children and cardiovascular disease [22]. In 2019, Sparrow et al. [23] highlighted that studies have discovered compelling evidence linking exposure to aircraft noise with cognitive impairment in children, particularly affecting their reading comprehension. Separately, in 2014, Babisch [24] reported that most studies consistently found evidence suggesting an increased risk of developing cardiovascular disease with higher noise levels. To aid understanding, a flow diagram illustrating the simplified chain reactions between transportation noise exposure and cardiovascular disease was created. Other than health issues, aircraft noise is known to affect housing prices as well [25,26]. Evidently, with hybrid work arrangement, managing aircraft noise can help improve the work environment for the stay-home population during office hours.

As residents, closing the windows during office hours is the most straightforward way to minimise aircraft noise from entering the living space. If soundproof windows are installed, further noise reduction can be achieved [27]. In view of exterior aesthetics, some property developers may

prohibit residents from changing the windows. Although residents can enjoy better indoor acoustic comfort after closing the windows, productivity may not increase owing to the lack of natural ventilation. Unless air conditioning is present, poor indoor thermal comfort can also adversely affect productivity [28]. Considering the growing interest in developing sustainable cities to combat climate change, natural ventilation is preferred over mechanical ventilation for energy conservation.

As small cities grow denser in population, the demand for residential buildings will naturally rise. Land scarcity may result in the development of residential buildings nearer to a busy airdrome. Instead, an existing airdrome may be redesigned and relocated elsewhere that is surrounded by residential buildings. Either way, residents may find difficulty maintaining concentration at work, affecting productivity. For urban planners, they must evaluate the potential repercussions resulting from the changes and collaborate closely with relevant authorities to effectively manage aircraft noise [29-33]. In Asia, the Kaohsiung International Airport (Taiwan) [34], the Gimpo International Airport (South Korea) [35], the Tengah Air Base (Singapore) [36], the Changi International Airport (Singapore) [37], and the Hangzhou Xiaoshan International Airport (China) [38] are examples with residential buildings found nearby.

Seeing how hybrid work arrangement has become a formal norm in more organisations, urban planners are now placing even more emphasis on exploring solutions that can manage aircraft noise in new and existing residential areas. To ensure efficient resource management, it is imperative to identify problematic regions in the neighbourhood before brainstorming for solutions. For existing neighbourhoods, residents can be engaged through surveys to garner their feedback. For example, in 2023, the Federal Aviation Administration [39] updated the National Sleep Study database with the latest survey findings. Residents who participated (400) were surveyed for 2 years to study the effects of nocturnal aircraft noise on their sleep. The findings helped inform authorities about the need for potential revisions to existing noise regulations. For new neighbourhoods under development, noise maps can be used. For assurance, site visits can also be conducted because there may be other physical factors present on-site - preserved infrastructures, for example - that affect the accuracy of the noise maps. Heinonen-Guzejev et al. [40] showed that noise maps are also applicable for existing neighbourhoods and can be used to validate survey findings.

A noise map is a form of data visualisation that provides urban planners with insights into the intensity and distribution of noise in a neighbourhood. To compute accurate noise maps, commercial software requires the user to define a plethora of input parameters. In most cases, some input parameters are unknown. As such, the user is required to complete the scenario by making informed assumptions, which may or may not affect the accuracy of the noise map. Also, because commercial software performs most computations in a black box, it is difficult to fully comprehend the assumptions made [41]. Considering that urban planners are mostly not specialised in acoustics, defining every input parameter can be a challenging task, not to mention time-consuming. Instead, urban planners rely on acoustic consultants to provide accurate noise maps. As acoustic consultants are often handling multiple projects, it may take a few weeks before urban planners receive the noise maps. Occasionally, while waiting, urban planners may need to quickly evaluate potential noise issues in the neighbourhood so that noise management strategies can be brainstormed in advance. Therefore, there is a need for urban planners to possess a simulation tool that does not have a steep learning curve and is able to easily produce noise maps based on the specific needs of local regulations.

Although not specifically developed with urban planners in mind, researchers have recognised the need for a simulation tool that offers more transparency and flexibility in producing noise maps resulting from aircraft operations. A notable example is the model (sonAIR) developed by the Swiss Federal Laboratories for Materials Science and Technology (Empa) [42-44]. The motivation behind the development stemmed from the necessity to generate noise maps arising from novel aircraft designs or updated flight procedures without the need for input data, such as the geometry of aircraft components, which may not be readily available.

In another example, Riboldi et al. [45] saw the need to develop a model that can produce noise maps resulting from new battery-powered aircraft designs. The model was developed based on ECAC Doc 29 [46-48]. Established by the European Civil Aviation Conference (ECAC), ECAC Doc 29 is widely regarded as one of the best practice models for producing noise maps resulting from aircraft operations. The Environmental Noise Directive published by the European Union [49] also recommends the utilisation of ECAC Doc 29. Based on the same best practice model, others have also implemented computation procedures to consider non-towered airports [50] and ground operations [51].

In our case, we have been internally developing a unified urban environmental modelling tool [52] that aims to help urban planners design more liveable and sustainable residential towns in an intuitive and quick manner. Setting

itself apart from commercial software, the modelling tool has the capability to seamlessly integrate a range of environmental factors, including wind flow, solar exposure, wind-driven rain, building energy usage, and outdoor noise. As a result, it can analyse the interdependencies and cumulative effects of these environmental factors on a given urban setting.

As discussed in earlier paragraphs, the rising demand for hybrid work arrangement and the steep learning curve of commercial software motivated us to include aircraft noise mapping as one of the features in the modelling tool. While commercial software can offer great flexibility in scenario creation, urban planners can benefit from automated processes to quickly evaluate potential noise issues in the neighbourhood so that noise management strategies can be brainstormed in advance. Based on ECAC Doc 29, we developed the package such that noise maps can be easily generated via simplified procedures and a reduced amount of input data, with acceptable accuracy in the results. These benefits distinguish our developed package from commercial software. However, we must stress that the results produced by our developed package are intended primarily for quick evaluation and should be regarded as approximate. Ultimately, it is advisable to validate the results through field measurement data and benchmarking with commercial software tailored for comprehensive noise calculations. This article aims to present how the aircraft noise mapping package was developed and benchmarked.

This article is structured in a sequential manner. Each section builds upon the previous one to provide a logical understanding of the whole research and development process. In Section 2, we present the development of the aircraft noise mapping package by discussing the methodology, algorithms, and data sources employed. Next, in Section 3, we present how the results were benchmarked against those obtained from the commercial software, SoundPLAN. Before concluding this article in Section 5, we discuss the main limitations of our developed package and the potential avenues for consideration as future work in Section 4.

2 Development of the aircraft noise mapping package

The aircraft noise mapping package consists of algorithms fully written in Python. Essential libraries include NumPy, pandas, SymPy, Matplotlib, and imageio. This section describes how the package was developed in the back-end (Sections 2.1-2.3) and presented in the graphical user interface (GUI) (Section 2.4).

2.1 Selecting the reference model

Aircraft noise prediction models can be classified into theoretical (or scientific) models and best practice models. Theoretical models are designed to estimate the absolute noise level of an aircraft that does not currently exist, accounting for unconventional configurations, new designs, or novel operating procedures. However, due to their proprietary nature, theoretical models may have limited accessibility for widespread use. Conversely, best practice models offer a more practical and user-friendly approach, making them suitable for users without extensive technical expertise. Best practice models prioritise providing users with a quick understanding of the noise distribution across a specific land area. It is worth noting that best practice models rely exclusively on measurements published by manufacturers, limiting their analysis to existing aircraft. Ang and Cui [22] recently published a review article that offers a more detailed background relating to this topic.

As summarised by Ang and Cui [22], notable examples of aircraft noise prediction models include DLR AzB, ECAC Doc 29, and ICAO Doc 9911. These models were developed by the German Aerospace Centre (DLR), the ECAC, and the International Civil Aviation Organisation (ICAO), respectively. Among these models, ECAC Doc 29 is widely used because its guidelines were partially incorporated into both DLR AzB and ICAO Doc 9911, serving as the foundation. Pertaining to language, both ICAO Doc 9911 and ECAC Doc 29 are published in English. Pertaining to availability, only ECAC Doc 29 is an open access resource. It relies on the Aircraft Noise and Performance (ANP) database [53], which is also free to access. Considering these factors, we selected ECAC Doc 29 as the reference that guided our development of the aircraft noise mapping package. Although ECAC Doc 29 consists of three volumes [46–48], only the second volume contains the guidelines for algorithm development.

2.2 Selecting the noise metric

There are two categories of noise metrics that quantify aircraft noise. They are single-event and cumulative noise metrics. For single-event noise metrics, commonly used examples include maximum noise level ($L_{\rm Amax}$) and sound exposure level ($L_{\rm AE}$). These metrics are used to describe the noise level of an individual flight event at a given receiver location. For cumulative noise metrics, commonly used examples include day-evening-night noise level ($L_{\rm den}$) and day-night noise level ($L_{\rm dn}$). These metrics consider multiple flight events over an extended period of time to assess the

overall noise impact at a given receiver location. Both single-event and cumulative noise metrics are generally A-weighted. Compared to other weightings, the A-weighting has been widely adopted because it adjusts the noise spectrum to account for the sensitivity of the human ear to the audio frequency range of 20 Hz to 20 kHz. A detailed discussion of the respective noise metrics can be found in the review article published by Ang and Cui [22].

Being a new development, the aircraft noise mapping package was designed to consider only single-event flights quantified by one noise metric. Naturally, only single-event noise metrics (L_{Amax} and L_{AE}) used in the ANP database can be selected. In ECAC Doc 29 Vol 1, it is discussed that nonspecialists may find it difficult to understand the concept of the L_{AE} noise metric compared to the L_{Amax} noise metric. Therefore, the L_{Amax} noise metric is typically favoured over the other noise metric. Keeping in mind that the unified urban environmental modelling tool is designed for users who are mostly not specialised in acoustics, it is of utmost priority to produce noise maps that can be easily understood. Considering these factors, we selected the L_{Amax} noise metric. Acknowledging the importance of supporting additional noise metrics tailored for typical urban planning scenarios, we can expand beyond the L_{Amax} noise metric at a later stage, as discussed in Section 4.1.

2.3 Designing the algorithm workflow

The aircraft noise mapping package consists of three modules that form the algorithm workflow (Figure 1). These modules were designed to operate sequentially, with the outputs of the first module serving as inputs for the second module and the outputs of the second module serving as inputs for the third module. Fundamentally, the first, second, and third modules fulfil the respective roles of the pre-processor, solver, and post-processor within the package. The following sections are dedicated to presenting the workflow of each module.

At this point, it is important to mention that this section does not cover every equation used in the developed package. They are well described in ECAC Doc 29 Vol 2. In this section, only those essential for understanding the algorithm workflow are discussed. It is also important to note that equations and parameters used in aviation are often expressed in imperial units. To be consistent with the literature, including ECAC Doc 29 Vol 2, this section adopts the same units to minimise the use of conversion constants that may otherwise cause unnecessary complications or make the equations appear unfamiliar. Despite this, since

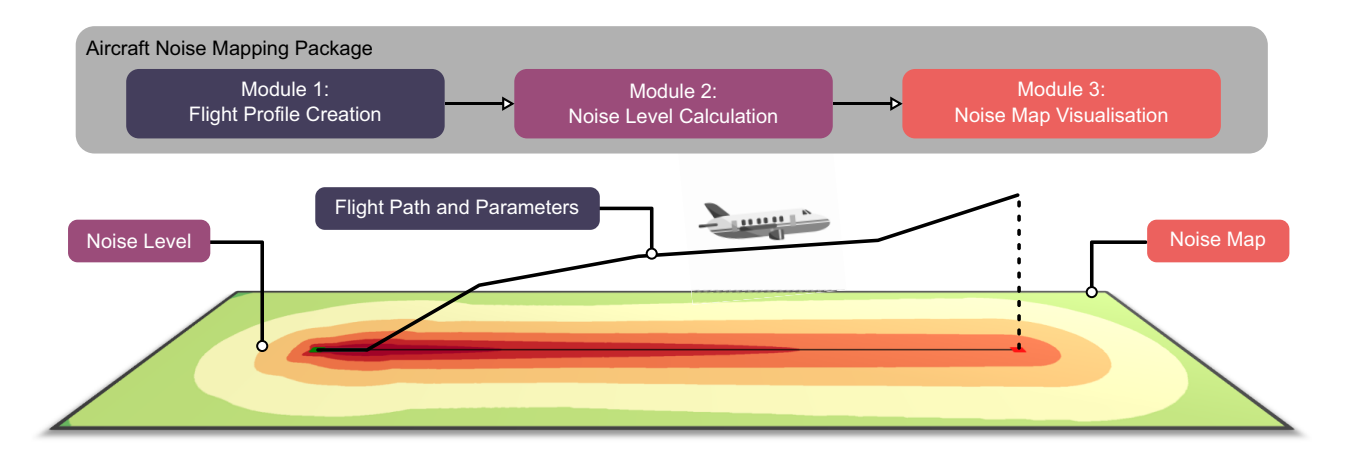


Figure 1: An overview of the aircraft noise mapping package consisting of three modules that form the algorithm workflow.

the modelling tool employs metric units as its default system of measurement, all results and quantities within the GUI are presented in metric units. Unless otherwise stated, the values of all variables can be obtained from the embedded ANP database.

2.3.1 Module 1: Flight profile creation

In the GUI, the user starts by selecting the aircraft of interest and specifying the flight type (departure or arrival) for the simulation. Although the ANP database provides datasets for more than 100 aircraft models, only 30 of them were integrated into the module. The datasets provide all modules with the essential information needed to compute the noise maps. The information includes the general specifications, engine coefficients, aerodynamic coefficients, flight procedures, and noise-power-distance (NPD) values of the aircraft.

Other than aircraft and flight type, the user may edit the default values of the parameters that define the reference condition of the aerodrome. The parameters include ambient air pressure, ambient air temperature, headwind, runway elevation, runway gradient, and runway length. The values of the first two parameters are given based on the International Standard Atmosphere at mean sealevel [54]. The values of the next three parameters are given based on those published by the manufacturers when they measured the engine coefficients [47]. In reality, wind conditions are rarely constant and can vary widely. For the sake of simplicity, ECAC Doc 29 Vol 2 recommends keeping the wind speed and direction constant regardless of altitude. If needed, the user can define a tailwind by entering a negative wind speed. The module will recognise the entry as a tailwind. Considering that the modelling tool will be largely used to study scenarios within Singapore, the default runway length is given as the length of the runways at Changi International Airport, which is the main airport of Singapore. This information reduces the time spent on literature search for the user. Finally, the default runway heading is provided based on the scenario in which the aircraft is departing eastward or arriving from the west. The runway heading is positive when specified clockwise from the magnetic north. A summary of the default values is shown in Table A1.

The back-end algorithm reads the user-input values and executes the relevant computations (Figure 2) to output the flight profile. The flight profile contains the flight path segmented according to the guidelines in ECAC Doc 29 Vol 2. Every segment is defined by one starting point (x_1, y_1, z_1) and one ending point (x_2, y_2, z_2) . At every point, it is assigned with the values of the performance parameters - corrected net thrust (CNT) and calibrated airspeed (CAS). The computational procedure is different between departure and arrival. For departure, the computational procedure starts on the runway and ends at a prescribed altitude. For arrival, the sequence of the computational procedure is reversed. Apart from this difference, many equations are not interchangeable between both flight types. To facilitate the discussion, the flight procedures are provided as supplementary information in Tables A2-A5. These default flight procedures represent a conservative scenario.

2.3.1.1 Takeoff ground roll

For departure, the first step (Tables A2 and A4) is to compute the flight profile when the aircraft is on the runway. which is between the brake release point and the takeoff point. In practice, it is common for the aircraft to stop completely at the brake release point and wait for takeoff

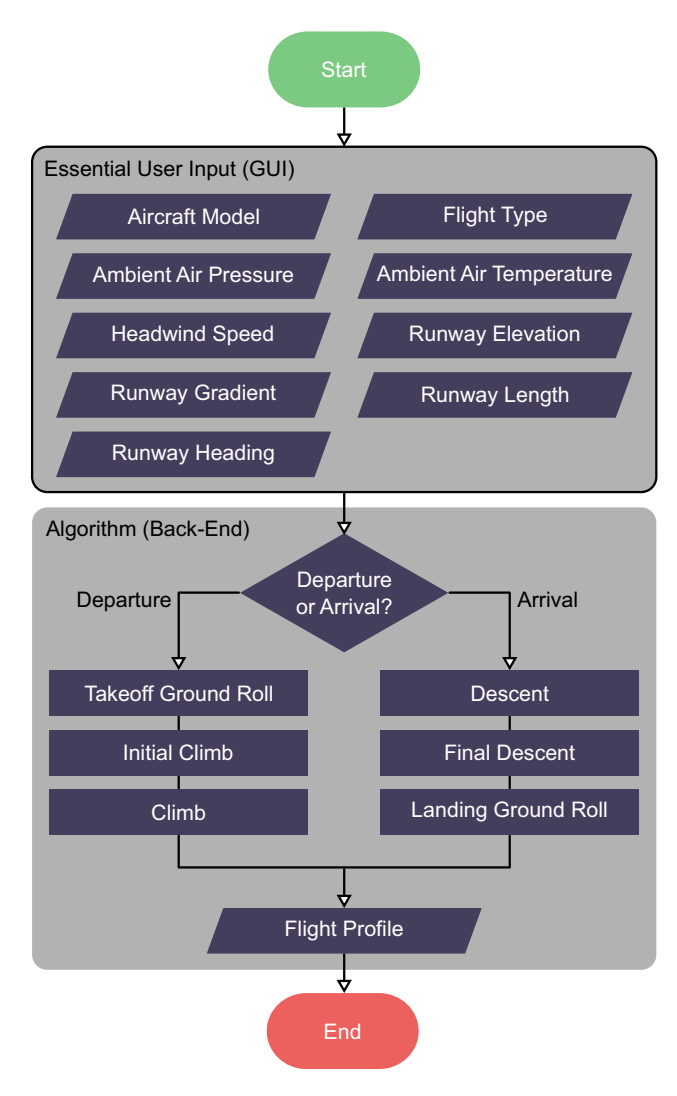


Figure 2: Flowchart of Module 1. The output (flight profile) contains the flight path segments, each defined by one starting point (x_1, y_1, z_1) and one ending point (x_2, y_2, z_2) along with the values of the performance parameters (CNT and CAS) at the respective points.

clearance. As such, the module will always assign 0 kt to the initial CAS of the step. At the takeoff point, the CAS is approximated using

$$V \approx C \cdot \sqrt{W}. \tag{1}$$

where C (kt/lb^{0.5}) denotes the aerodynamic coefficient at the prevailing flap setting and W (lb) denotes the maximum gross takeoff weight of the aircraft. Knowing the initial and final CAS of the step, the module can then determine the number of segments needed to divide the flight path such that the change in CAS per segment must not exceed 20 kt [47]. This relationship is expressed by

$$N_{\text{seg}} = \text{int}(1 + |V_2 - V_1|/20),$$
 (2)

where V_2 and V_1 (kt) denote the final and initial CAS of the step, respectively.

The length of the flight path is described by the ground distance covered. Specific to the takeoff ground roll, the following equation is used:

$$\Delta s = \frac{B \cdot \theta \cdot (W/\delta)^2}{N_{\text{eng}} \cdot (F_n/\delta)},$$
 (3)

where B (ft/lb) denotes the coefficient that represents the relationship between the aircraft, the flap setting, and the default headwind; θ denotes the ratio of the ambient air temperature at the prevailing altitude to that at mean sea-level; δ denotes the ratio of the ambient air pressure at the prevailing altitude to that at mean sea-level; $N_{\rm eng}$ denotes the number of engines; W/δ (lb) denotes the corrected weight; and F_n/δ (lb) denotes the CNT per engine. Subsequently, the ground distance covered per segment is determined using

$$\Delta s_k = \frac{(2k-1) \cdot \Delta s}{N_{\text{seg}}^2} \quad \text{for } 1 \le k \le N_{\text{seg}}, \tag{4}$$

where k denotes the segment number. At this point, the coordinates of the flight path segments are obtained.

The module proceeds to compute the performance parameters (CAS and CNT) for every segment. ECAC Doc 29 Vol 2 specifies that the performance parameters are assumed to increase linearly from one segment to another during the takeoff ground roll. As the initial and final CAS of the step are already known (equation (2)), the module only needs to compute the change in CAS per segment using the following equation:

$$\Delta V = \frac{V_2 - V_1}{N_{\text{seg}}},\tag{5}$$

where the same applies for the change in CNT per segment, replacing V with F_n/δ . Before this is possible, the module must compute the initial and final CNT of the step. At the brake release point, the CNT is equal to the maximum sealevel static thrust. At the takeoff point, the CNT is computed according to the engine type.

The approach to computing the CNT for one engine type may not apply for another engine type. The module can support turboprop, turbojet, and turbofan engines, which are the common engine types found in local aerodromes. For turboprop engines, the CNT is computed using

$$F_n/\delta = \frac{326 \cdot \eta \cdot P_n \cdot \sqrt{\sigma}}{V \cdot \delta},\tag{6}$$

where η denotes the propeller efficiency; P_n (hp) denotes the net propulsive power; and σ denotes the ratio of the ambient air density at the prevailing altitude to that at mean sea-level. For turbojet and turbofan engines, the CNT is computed using

$$F_n/\delta = E + F \cdot V + G_A \cdot z + G_B \cdot z^2 + H \cdot T_z, \tag{7}$$

where z (ft) denotes the altitude; E (lb) denotes the engine thrust constant; T (°C) denotes the ambient air temperature; F (lb/kt), G_A (lb/ft), G_B (lb/ft²), and H (lb/°C) denote the different engine thrust coefficients. Note that both equations can be used to determine the CNT at any point on the flight path, not just at the takeoff point, by substituting the prevailing values of the variables.

2.3.1.2 Initial climb

Once the aircraft is airborne, the module computes the flight profile specific to the initial climb, which extends from the takeoff point to the point where the altitude is 1,000 ft (Tables A2 and A4). Here, the aircraft operates at a constant speed. Therefore, the module assigns the final CAS the same value of the initial CAS (i.e., $V_2 = V_1$). For every segment, the initial and final CNT are computed using either equation (6) or (7).

Unlike the takeoff ground roll, the approach to segmenting the flight path of the initial climb is based on a list of reference altitudes given in ECAC Doc 29 Vol 2. Established from past research, the approach was shown to produce reliable noise predictions when the aircraft is close to the ground. In this way, the change in lateral attenuation per segment is kept within 1.5 dB. Knowing the initial and final altitudes of every segment and the number of segments, the ground distance covered per segment is estimated using

$$\Delta s_k = \frac{z_{2,k} - z_{1,k}}{\tan \overline{y}} \quad \text{for } 1 \le k \le N_{\text{seg}}, \tag{8}$$

where \overline{y} (rad) denotes the average climb angle of the step computed using

$$\overline{y} = \arcsin \left[K \cdot \left(N_{\text{eng}} \cdot \frac{\overline{F_n/\delta}}{\overline{W/\delta}} - \frac{R}{\cos \varepsilon} \right) \right],$$
 (9)

where R denotes the ratio of the drag coefficient to the lift coefficient of the aircraft at the prevailing flap setting; ε (rad) denotes the bank angle; and K denotes the speeddependent constant. If $\overline{V} \le 200$ kt, K = 1.01. Else, K = 0.95. At this point, the coordinates of the flight path segments are obtained.

2.3.1.3 Climb

For the rest of the climb, the aircraft accelerates from time to time until the maximum allowable speed is attained. After

which, the aircraft maintains the same speed until it reaches 10,000 ft in altitude – the highest point of interest for noise predictions. The module determines if the aircraft is accelerating or not from the flight procedures (Tables A2 and A4).

If the step involves acceleration, the module will check whether there is a change in thrust rating from the previous step. If the check returns true, the module will implement a transition step for thrust cutback immediately after the previous step. Examples are given by the fourth step in Table A2 and the third step in Table A4. In practice, implementing thrust cutback can help extend engine life and reduce noise pollution. The guideline [47] specifies that the transition step should take place over a ground distance of 1,000 ft. For the sake of simplicity, the aircraft is assumed to operate at a constant speed. Hence, segmenting the flight path is not needed. The cutback CNT is computed using

$$F_n/\delta_2 = \frac{W/\delta_2}{N_{\text{eng}} - 1} \cdot \left[\frac{\sin(\arctan G')}{K} + \frac{R}{\cos \varepsilon} \right], \quad (10)$$

where G' denotes the engine-out climb gradient. The module then assigns the cutback CNT to the initial CNT of the acceleration step. Finally, the altitude at the end of the transition step is computed using equation (8).

If the check returns false, the module will enter an iterative loop designed to determine the final altitude of the step. Examples are given by the sixth step in Tables A2 and A4. In the first iteration, the final altitude is estimated by adding 250 ft to the initial altitude, as specified in ECAC Doc 29 Vol 2. Using this initial estimate, the objective is to re-estimate the final altitude from the flight path and the performance parameters computed using

$$z_2' = z_1 + \Delta s \cdot G/0.95,$$
 (11)

where G denotes the climb gradient of the step and Δs denotes the ground distance covered computed using

$$\Delta s = \frac{1.36 \cdot (V_2^2/\sigma_2 - V_1^2/\sigma_1)}{a_{\text{max}} - 32.17 \cdot G},$$
(12)

where a_{max} (ft/s²) denotes the maximum acceleration of the step determined using

$$a_{\text{max}} = 32.17 \cdot \left[N_{\text{eng}} \cdot \frac{\overline{F_n/\delta}}{\overline{W/\delta}} - \frac{R}{\cos \varepsilon} \right].$$
 (13)

In equations (11) and (12), the climb gradient is approximated using

$$G \approx \frac{\text{ROC}}{50.64 \cdot (V_1/\sqrt{\sigma_1} + V_2/\sqrt{\sigma_2})},\tag{14}$$

where ROC (ft/min) denotes the rate of climb. To end the iterative loop, the absolute difference between the initial estimate and the re-estimated final altitude (equation (11)) must be within 3 ft. If this condition is not met, the module will begin a new iteration by adding 3 ft to the initial estimate. It is stated in ECAC Doc 29 Vol 2 that the value to use depends on the decision of the developer in striking a balance between accuracy and computational speed. In our case, we decided on 3 ft because it corresponds to about 1 m. For every iteration, the initial estimate is obtained from

$$Z'_{2,M} = \underbrace{Z_1 + 250}_{M=1} + \underbrace{3 \cdot (M - 1)}_{M \ge 2},$$
 (15)

where M denotes the iteration count starting from 1. Once the iteration ends, the ground distance covered per segment is computed using

$$\Delta s_k = \frac{2 \cdot \Delta s}{N_{\rm seg}} \cdot \frac{V_1 + \Delta V \cdot (k-0.5)}{V_1 + V_2} \quad \text{for } 1 \le k \le N_{\rm seg}, \quad (16)$$

where N_{seg} and Δs are obtained from equations (2) and (12), respectively. Subsequently, the initial and final altitudes of every segment are obtained via linear interpolation. The initial and final CNT are computed using either equation (6) or equation (7).

Finally, if the step involves no acceleration, the module will use equations (8) and (9) to compute the flight path and either equation (6) or equation (7) to compute the initial and final CNT where applicable. As the CAS stays the same throughout the step, segmenting the flight path is not required. Examples are given by the fifth step in Tables A2 and A4.

2.3.1.4 Descent

For arrival, noise predictions are concerned with the altitude of 6,000 ft and below. The aircraft must decelerate to the required CAS by the time it enters the final descent at 1,000 ft. Deceleration can take place during either descending or level flight. Examples are given by those before the fourth step in Table A3 and those before the sixth step in Table A5.

If the step requires the aircraft to decelerate and descend concurrently, the module will first compute the ground distance covered using equation (8). This output is then substituted into equation (16), along with the initial and final CAS, to determine the ground distance covered per segment. The number of segments is obtained from equation (2). If the step requires the aircraft to decelerate at a constant altitude, covering a certain ground distance, the module will only need to determine the segment count and the ground distance covered per segment. At this point, the coordinates of the flight path segments are obtained.

Finally, the module computes the initial and final CNT of every segment according to the engine type. For turbojet

and turbofan engines, equation (7) is used. For turbofan engines, the following equation is used:

$$F_n/\delta = \frac{W/\delta}{N_{\text{eng}}} \cdot [R \cdot \cos \overline{y} + \sin \overline{y} + a_{\text{max}}/32.17], \quad (17)$$

where W (lb) denotes the maximum gross landing weight of the aircraft and a_{max} (ft/s²) denotes the maximum deceleration of the step computed using

$$a_{\text{max}} = \frac{\cos \overline{y}}{2 \cdot \Delta s} \cdot \left[\frac{V_2^2}{\sigma_2} - \frac{V_1^2}{\sigma_1} \right] + \frac{8}{\Delta s} \cdot \left[\frac{V_1}{\sqrt{\sigma_1}} - \frac{V_2}{\sqrt{\sigma_2}} \right]. \quad (18)$$

The initial and final CAS of every segment are determined via linear interpolation.

2.3.1.5 Final descent

At an altitude of 1,000 ft, the aircraft commences its final descent, which ends at the point when the aircraft is above the landing threshold of the runway (i.e., landing threshold point). Examples are given by the fourth step in Table A3 and the sixth step in Table A5. The approach to segmenting the flight path is the same as that for the initial climb, using the list of reference altitudes given in ECAC Doc 29 Vol 2. Using equation (8), the ground distance covered per segment is determined. At this point, the coordinates of the flight path segments are obtained.

As the CAS is kept constant, every segment is assigned the same value at the starting point and the ending point. Regardless of engine type, the initial and final CNT of every segment are computed from equation (9) by having $\overline{F_n/\delta}$ as the subject with K=1.03.

2.3.1.6 Landing ground roll

In this last part of the arrival, the flight profile is computed from the landing threshold point to the taxiing point (e.g., last three steps in Tables A3 and A5). The taxiing point refers to the instance when the CAS of the aircraft reaches 30 kt. In practice, the aircraft must complete its rapid deceleration to the taxiing speed after covering a certain ground distance (aircraft-specific) from the touchdown point. This distance is also known as the stop distance. In some situations, it is runway-specific. Examples are given by the sixth step in Table A3 and the eighth step in Table A5.

From the landing threshold point to the touchdown point, the ground distance covered and the average descent angle are given in the flight procedures. Using equation (8), the altitude of the aircraft at the landing threshold point can be estimated. During this period, the performance

parameters remain unchanged. Therefore, segmenting this part of the flight path is not needed.

After the touchdown point, the aircraft usually relies on thrust reversal to decelerate rapidly over the stop distance. As the process of thrust reversal varies among aircraft, the module adopts the generalised approach as proposed in ECAC Doc 29 Vol 2. At the moment when the aircraft covered 10% of the stopping distance, the CNT is at 20% of the maximum sea-level static thrust. For the remaining 90% of the stop distance, the CNT is gradually reduced from 20 to 10% of the maximum sea-level static thrust. Equation (16) is used to segment the flight path between the touchdown point and the taxiing point. At this point, the coordinates of the flight path segments are obtained. Finally, the module computes the performance parameters at the starting and ending points of every segment via linear interpolation.

2.3.2 Module 2: Noise level calculation

Now that the flight profile (noise source) of the aircraft is known, the second module helps create the horizontal calculation plane defined by a rectangular or square grid of nodes (noise receivers). The purpose of the module is to return the maximum noise level ($L_{\rm Amax}$) at every node with respect to the flight event. Figure 3 shows the flowchart of the module.

In the GUI, the user may choose to provide inputs for up to four parameters that the module uses to define the calculation plane. Otherwise, the user can skip the entries by accepting the default values (Table A1). The grid size specifies the lateral distance between the nodes. The smaller the grid size, the higher the sensitivity of the noise map. The altitude specifies the positive vertical distance of the plane relative to the runway. The GUI displays the last parameter (lateral coverage factor or plane corners) based on the chosen plane type (automatic or manual). For the automatic plane type, the user may specify the lateral coverage factor that determines how large the grid is relative to the bounding box of the ground track. This plane type is useful for obtaining an overview of the noise distribution over an area encompassing the flight path. For the manual plane type, the user must specify two sets of coordinates (x, y) that define the bottom left and top right corners of the grid. This option is suitable for general usage to study noise distribution in a user-defined region of interest.

In the back-end, the user-input values are used to create the grid of nodes that form the calculation plane. Together with the flight profile (from Module 1), the spatial information of the nodes is passed to a nested loop designed for noise calculations. The nested loop consists of one outer

for loop (for each flight segment) and one inner for loop (for each node). In each inner loop, the module must first compute the spatial relationship between the node and the flight segment to determine whether the node is in front of, behind, or alongside the flight segment, and whether the node is facing the left side, right side, or bottom of the flight segment. This information is essential for the module to appropriately correct the NPD value retrieved from the embedded ANP database, leading to the nodal noise level.

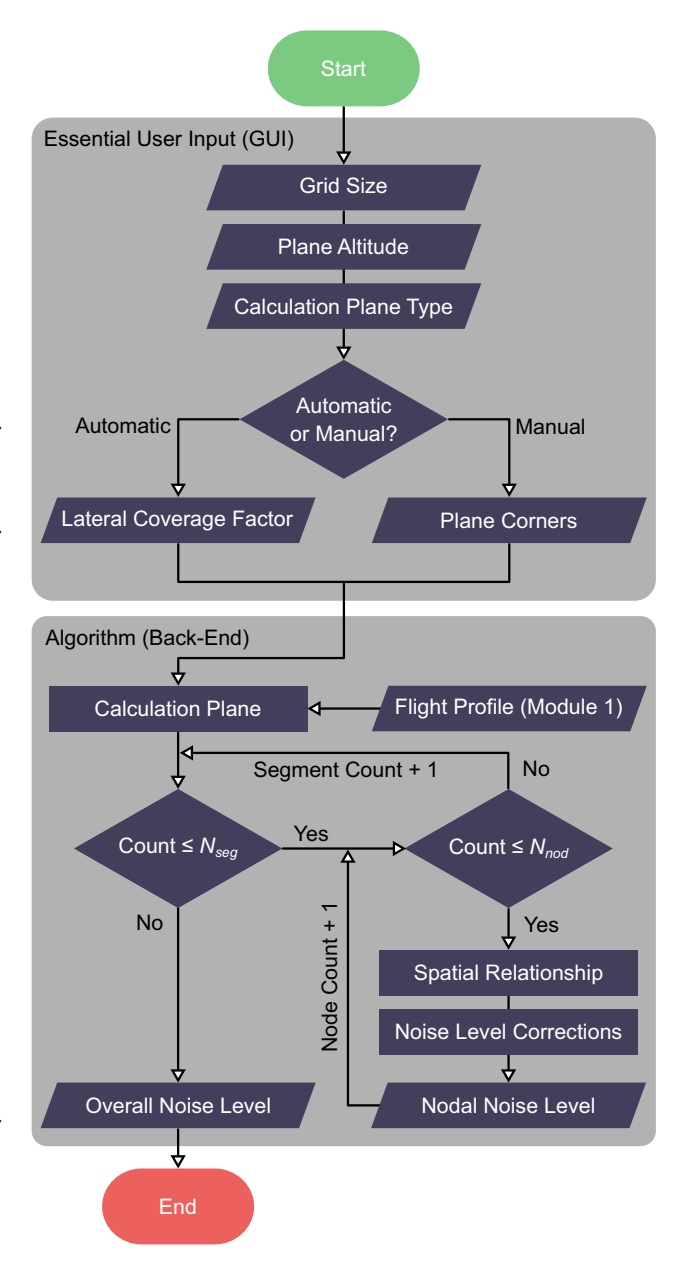


Figure 3: Flowchart of Module 2. The output (overall noise level) contains the coordinates (x, y, z) and the maximum noise level $(L_{\rm Amax})$ from all nodes on the grid of the calculation plane. $N_{\rm seg}$ and $N_{\rm nod}$ denote the number of flight segments and nodes, respectively.

Every NPD value corresponds to the noise level measured at the receiver for a given CNT of the aircraft and its direct distance to the receiver. Aircraft manufacturers would perform the measurements using different noise metrics under the reference condition of the aerodrome. Specific to the $L_{\rm Amax}$ noise metric, the nodal noise level is calculated using

$$L = L_{\text{NPD}} + \underbrace{\Delta_Z + \Delta_I + \Delta_B - \Lambda_L}_{\text{Correction Terms}},$$
 (19)

where L_{NPD} (dBA) denotes the retrieved NPD value; Δ_{Z} (dBA) denotes the correction that accounts for the difference in acoustic impedance between the reference condition and the actual condition of the aerodrome; Δ_I (dBA) denotes the correction that accounts for the change in lateral directivity influenced by wave interaction between the solid surfaces and the aerodynamic flow fields of the aircraft: Δ_R (dBA) denotes the correction that accounts for the directivity of engine noise behind the aircraft during the takeoff ground roll; and Λ_L (dBA) denotes the correction that accounts for lateral attenuation over distance. More details on the correction terms can be found in ECAC Doc 29 Vol 2. Once the noise levels are calculated for the grid of nodes with respect to the current flight segment (i.e., inner loop ends), the module proceeds to repeat the inner loop with respect to the next flight segment. The nested loop ends after the last flight segment is considered.

Before the computational procedure ends, the module returns the overall noise level ($L_{\rm Amax}$) at every node by extracting the maximum value of the nodal noise levels calculated for all flight segments. To elaborate, if 20 segments are involved, 20 noise levels will be calculated at the same node. The maximum value of the 20 noise levels will then be used as the overall noise level. As the user may be interested to study the noise distribution specific to the position of the aircraft, the module can also return the segment noise levels. All returns are saved to a comma-separated value (CSV) file, which will be used as the input in the next module.

2.3.3 Module 3: Noise map visualisation

Module 3 provides the user with results visualisation in the form of noise maps, which are available in two types (elaborated later). Figure 4 shows the flowchart of the module.

In the GUI, the user must import the results (CSV file from Module 2) so that the back-end has datasets to process into noise maps. The remaining entries are optional to fill. Under map layout settings, the user may specify the contour range, contour interval, and aspect ratio. Additionally, the user may toggle between displaying and hiding the

runway and the flight path in the noise map. Otherwise, the user can skip the entries by accepting the default settings. The last entry (map type) is an either/or radio button that the module uses to determine the type of noise map (overall or positional) that should be presented for results visualisation.

In the back-end, the file generators are the core algorithms that process the user-input values and results into noise maps. The overall and positional noise maps are generated as a portable network graphics (PNG) file and a graphics interchange format (GIF) file, respectively. The overall noise map shows the noise distribution ($L_{\rm Amax}$) resulting from the combined impact of the flight event. For this map type, the module plots it directly from the results file without any processing. The positional noise map shows the instantaneous noise distribution ($L_{\rm Amax}$)

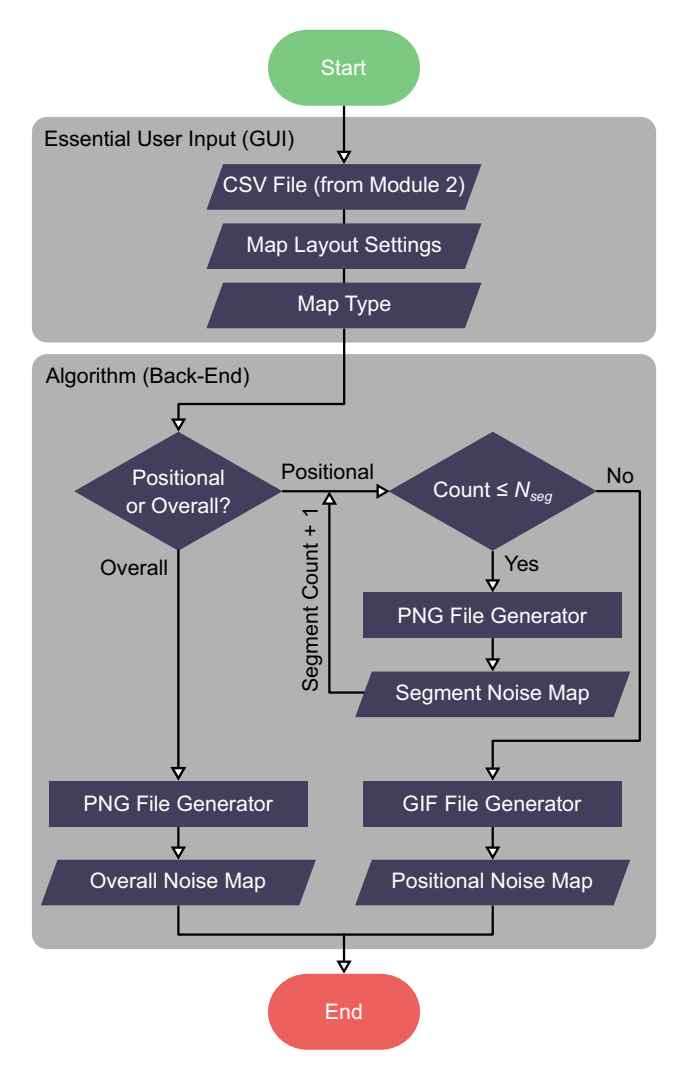


Figure 4: Flowchart of Module 3. All visualisations (overall and positional noise maps) are saved as their respective file formats in the working directory and then displayed in the GUI.

with respect to the position of the aircraft (represented by flight segments). To a layperson, the positional noise map is like a time-dependent noise map. However, considering the absence of a time component, labelling them as timedependent noise maps might not be appropriate. For this map type, the user-input values are first processed in a for loop designed to generate one noise map for every flight segment (i.e., position of the aircraft). Subsequently, the GIF file generator consolidates all of the noise maps into the animated positional noise map.

2.4 Simplifying the GUI workflow

As the GUI was developed by another team (see acknowledgements), it is beyond the scope of this article to discuss the front-end aspects in great detail. Here, the GUI specific to the aircraft noise mapping feature is briefly described for the sake of completeness. However, we are unable to disclose a screenshot of the GUI owing to sensitivity concerns.

To enhance user experience, each feature in the modelling tool was designed to follow the same four-step workflow: Model, Environment, Simulate, and Result. This design principle enables users to easily familiarise themselves with the GUI when switching between features, which include aircraft noise mapping. To enhance user focus, the modelling tool minimises GUI clutter by showing only the essential menus and buttons.

On the right side of the GUI, a floating pane with four tabs (one for every step) is presented to the user. The tabs are sequentially arranged to guide the user through the four-step workflow. User inputs specific to Modules 1 and 2 are listed under either the Model tab or the Environment tab. For user inputs specific to Module 3, they are listed under the Result tab. Finally, under the Simulate tab, the user is presented with a button to run the simulation for the created scenario.

3 Benchmarking of the results with **SoundPLAN**

It is important to highlight that the intention of benchmarking is not to determine which modelling tool is more superior than the other. The intention is also not to assess which modelling tool has a faster computational speed. As our unified urban environmental modelling tool emphasises ease of use by non-specialists, the key priority is to ensure that reliable results can be generated. Hence, the intention of benchmarking is to assess whether our developed package can provide reliable results by comparing them against those obtained from the commercial software, SoundPLAN (version 8.2).

Although benchmarking was done for many different scenarios, this section limits the discussions to two pairs of essential scenarios, each considering one aircraft model departing and arriving. This section starts by describing how the scenarios were created (Section 3.1) before moving on to discuss the results, which include benchmarking of the flight profiles (Section 3.2) and the overall noise maps (Section 3.3).

3.1 Creating the scenarios

In each pair of scenarios, one aircraft model (C-130 or 737-8 MAX) was considered. In every scenario, the flight type was either departure or arrival. The four scenarios were created to address the computational differences between engine types and between flight types (elaborated in Section 2). Apart from this reason, the C-130 turboprop aircraft and the 737-8 MAX turbofan aircraft were chosen for their operational presence in the aerodromes of Singapore.

As the computational procedure for handling turning flight paths has not been standardised [47], discrepancies may be expected when comparing results obtained from different modelling tools. To address this issue, a straight flight path was specified in all scenarios with the aircraft operating based on the default flight procedures (Tables A2-A5). The remaining parameters specific to Module 1 were kept at the default values (Table A1), ECAC Doc 29 Vol 2 recommends that the start of the runway should be set as the point of origin (x = 0, y = 0, z = 0). This recommendation was fulfilled in the back-end whenever a scenario was created.

Considering that the scenarios were meant for benchmarking, the calculation plane in every scenario was set to automatic. As elaborated in Section 2.3.2, the automatic plane type allows the back-end to define the most appropriate size of the plane that can encompass the flight event. To expand the coverage, the lateral coverage factor was set to 0.5 instead of the default value. The remaining parameters specific to Module 2 were kept at the default values (Table A1).

In SoundPLAN, many reference models (Section 2.1) are supported. Before any scenario can be created, ECAC Doc 29 must be selected as the reference model right after launching the software. Subsequently, the user must navigate a series of pop-up windows to select the aircraft model, specify the flight type, define the flight path, and assign the flight procedures. Unlike our developed package, the user is required to manually set the point of origin by entering the coordinates relative to the centre of the aerodrome.

SoundPLAN also offers limited capability to automatically define the calculation plane. The user must enter the coordinates of the four corners, which are again relative to the centre of the aerodrome. Otherwise, the placement and size of the plane can only be estimated by using the mouse to click and drag within the viewport. Hence, the user may spend a considerable amount of time to get the coordinates right. While SoundPLAN unquestionably offers great flexibility in scenario creation, urban planners can benefit from automated processes to quickly evaluate potential noise issues in the neighbourhood. This is where our developed package comes into play.

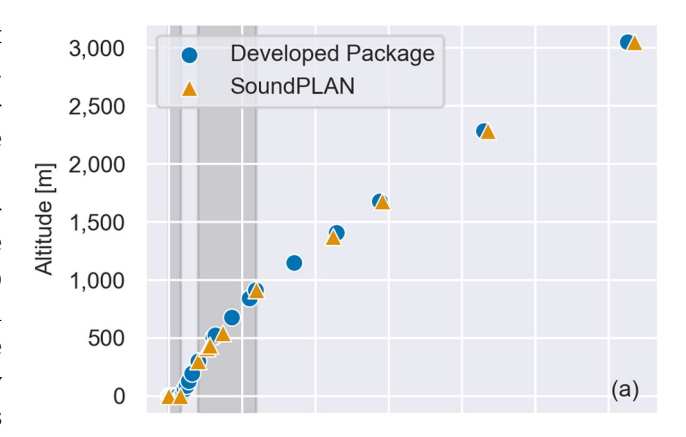
3.2 Benchmarking the flight profiles

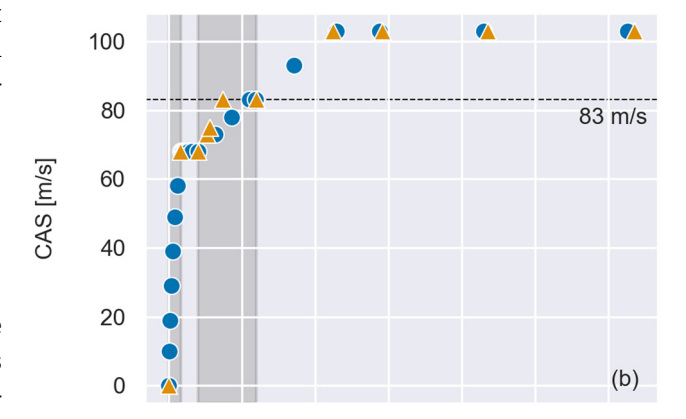
Being modular, we were able to assess the reliability of the output produced by Module 1 before transmitting it as input to Module 2. This approach streamlined the trouble-shooting process by allowing us to isolate and investigate any potentially problematic codes that could be contributing to the observed discrepancies. Here, we present the results in two sections to differentiate between turbo-prop (Section 3.2.1) and turbofan (Section 3.2.2) aircraft. For ease of interpretation, the results are presented in metric units.

In the results, we will see that our developed package produced more data points than SoundPLAN. This is because SoundPLAN could only produce data points at critical positions of the aircraft, mainly at the start and end of each step in the flight procedures. Intermediate data points were not disclosed. In contrast, our developed package could produce data points at the start and end of each segment, giving the user a comprehensive view of the results. In view of this difference, discrepancies can only be quantitatively discussed at the common data points. Negative percentages indicate underestimation, positive percentages indicate overestimation, and a discrepancy of 0% indicates an exact match.

3.2.1 Turboprop aircraft (C-130)

Figures 5 and 6 show the departure and arrival flight profiles, respectively, obtained from our developed package and SoundPLAN. A subplot is dedicated to





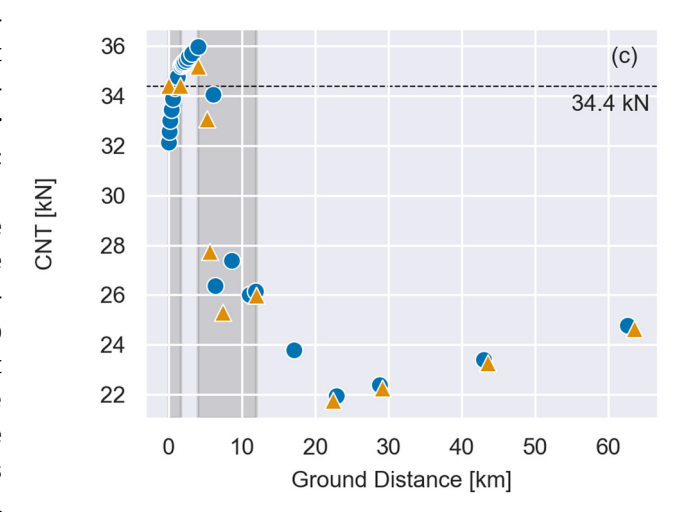


Figure 5: Departure flight profiles of the C-130 turboprop aircraft obtained from our developed package and SoundPLAN, showing (a) altitude, (b) CAS, and (c) CNT vs ground distance. Smaller shaded region denotes the takeoff ground roll. Larger shaded region denotes the start of the third step to the end of the fourth step in the flight procedures (Table A2).

every parameter (altitude, CAS, and CNT) to illustrate their changes relative to ground distance. In both figures, it can be observed that our developed package

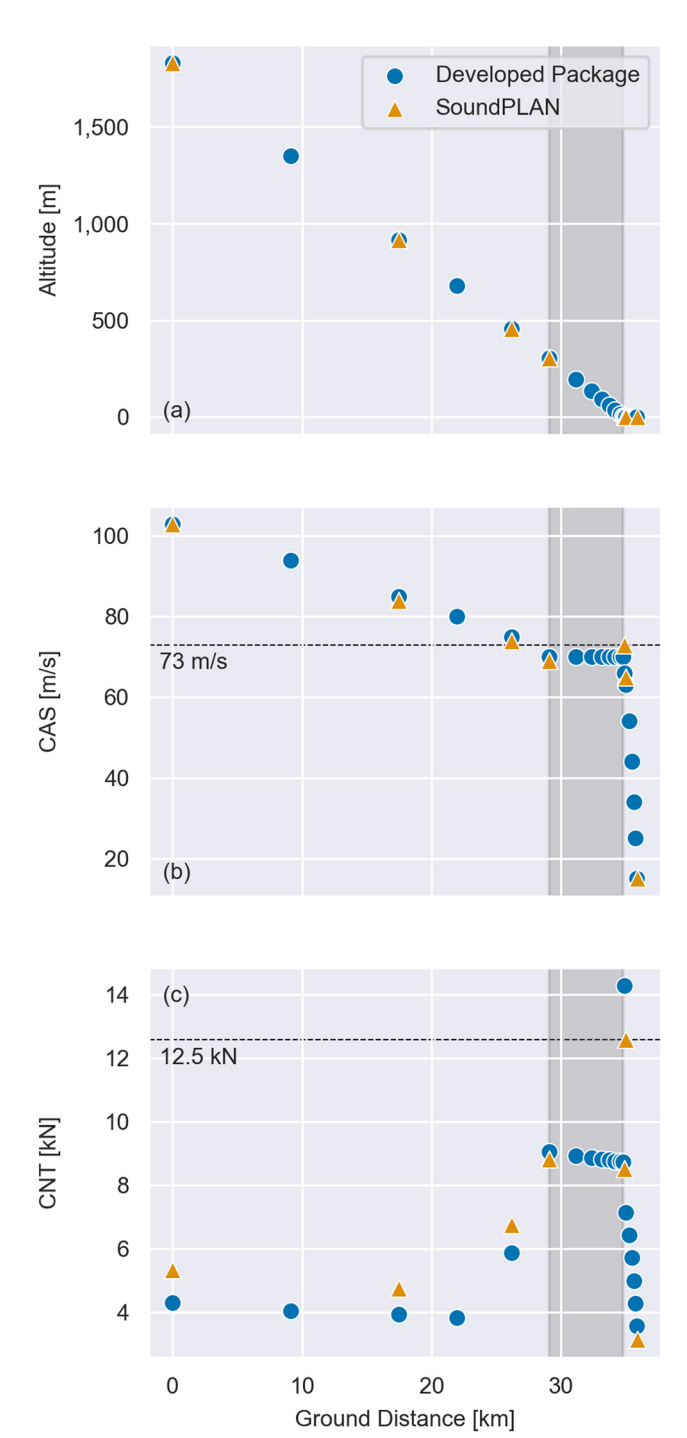


Figure 6: Arrival flight profiles of the C-130 turboprop aircraft obtained from our developed package and SoundPLAN, showing (a) altitude, (b) CAS, and (c) CNT vs ground distance. Shaded region denotes the final descent.

could produce results comparable to the benchmark in scenarios involving turboprop aircraft.

Specific to departure, the data points for altitude, ground distance, and CAS deviated from the benchmark over a range of -7.1 to 15.9%, 0 to 25.4%, and -6.2 to 0%,

respectively (Figure 5a and b). Large discrepancies were observed between the third and fourth steps of the flight procedures (Table A2). This observation might be attributed to the differences in how the iterative loops (Section 2.3.1.3) were coded compared to SoundPLAN. Also, in our developed package, the transition step for thrust cutback (Section 2.3.1.3) was assumed to take place at a constant speed. In SoundPLAN, the aircraft was assumed to accelerate instead, explaining why the aircraft arrived at 83 m/s earlier (Figure 5b). As specified in ECAC Doc 29 Vol 2, either way is valid and should not significantly affect the noise map, which we will see in Section 3.3. If the outliers were excluded, the data points for the respective parameters would deviate from the benchmark over a narrower range. For altitude, it would be 0-2.6%. For CAS, it would be -0.2to 0%. For ground distance, it would be -1.4 to 7.1% in which the upper limit is now caused by the difference in CNT during the takeoff ground roll.

The data points for CNT deviated from the benchmark over a range of -6.7 to 8.3% (Figure 5c). If the outliers were also excluded based on the above justifications, the range would become -6.7 to 2.3%. The upper and lower limits are now attributed to the difference in assumptions made to compute the CNT. In practice, the CNT is derated by 10-20% throughout the flight to prolong engine life and reduce noise emission [47]. As noise emission increases with CNT, our developed package adopts a conservative approach by considering the lower limit (10%). At the brake release point, the CNT was derated to 90% (32.1 kN) of the maximum sea-level static thrust (35.7 kN). At the takeoff point, the CNT was computed from equation (6) and derated to 90% (35.2 kN). In SoundPLAN, the CNT was treated as constant (34.4 kN) throughout the takeoff ground roll. Our investigations uncovered that the constant value was obtained by substituting the net propulsive power ($P_n = 3,575$ hp) meant for climbing instead of takeoff into equation (6). If the net propulsive power $(P_n = 4, 205)$ hp) meant for takeoff was substituted, the data points would agree well. Consequently, the data points for CNT and ground distance would deviate from the benchmark over a narrower range. For CNT, it would be 0.1-0.9%. For ground distance, it would be -1.4 to 2.2%.

Specific to arrival, the data points for altitude were in excellent agreement with the benchmark, having no discrepancies (Figure 6a). The data points for ground distance and CAS deviated from the benchmark over a range of -0.9 to 0% and -4.1 to 1.9%, respectively (Figure 6b). For CAS, the lower limit (-4.1%) was caused by the higher CAS (73 m/s) obtained from SoundPLAN. Referring to the flight procedures (Table A3), the CAS should either decrease or stay constant from one step to another. This behaviour is

consistent with the data points obtained from our developed package. Being a black box, it was technically challenging to determine the root cause of why SoundPLAN produced the data point at 73 m/s. Hence, our developed package preserved the recommendations in the flight procedures. Otherwise, smaller discrepancies would be observed (0–1.9%).

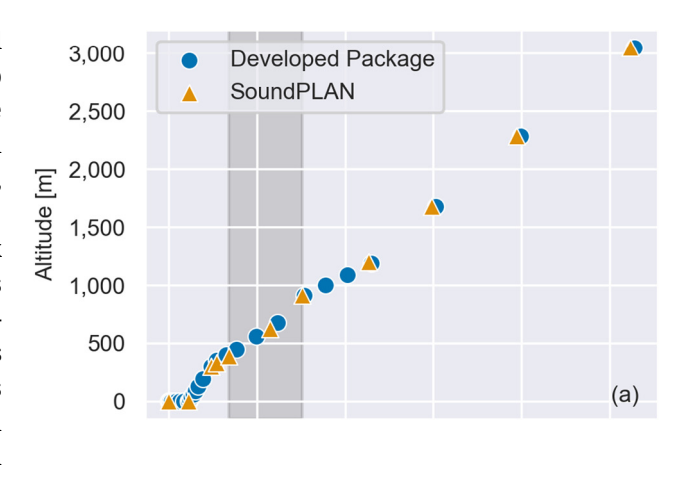
For CNT, the data points deviated from the benchmark over a range of –19.3 to 13.7%. The first three data points before the final descent contributed to the negative discrepancies. Similar to the case for departure, investigations were conducted to uncover the exact values of all variables that SoundPLAN had substituted into equations (17) and (18). Owing to the troubleshooting challenges associated with a black box, a different perspective was taken. As the values of all variables were given in the flight procedures (Table A3), assurance was established by ensuring that the correct values were retrieved and substituted into the correct equations. Furthermore, the data points showed strong overall agreement in trend. Therefore, our developed package was deemed reliable in producing data points before the final descent.

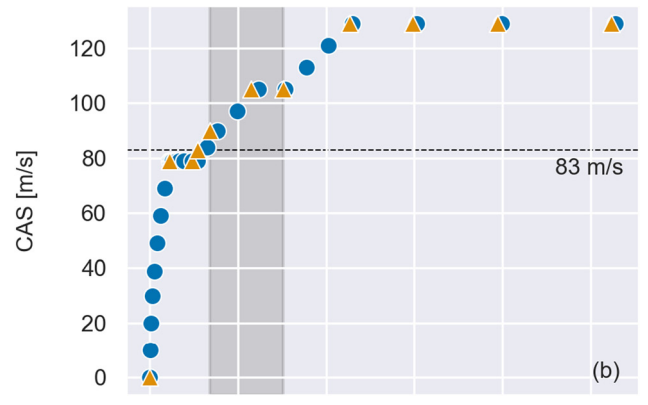
The data points after the final descent contributed to the positive discrepancies. Small discrepancies (2.6%) were observed for the two data points at the start of the final descent and at the touchdown point. The main contributors to the discrepancies (13.7%) were the data points at the thrust reversal point and the taxiing point. For both data points, our developed package computed the CNT according to the recommendations in the flight procedures (Table A3). As such, the CNT at the thrust reversal point should be 40% (14.3 kN) of the maximum sea-level static thrust (35.7 kN). At the taxiing point, the CNT should be 10% (3.6 kN) of the maximum sea-level static thrust (35.7 kN). Our investigations uncovered that SoundPLAN computed the respective CNT values using 35% (12.5 kN) and 8.8% (3.1 kN) instead of 40% and 10%. As the latter pair is also recommended in ECAC Doc 29 Vol 2 as a generalised approach, our developed package maintained consistency with the recommendations in the flight procedures.

3.2.2 Turbofan aircraft (737-8 MAX)

Presented in the same manner, Figures 7 and 8 show the departure and arrival flight profiles, respectively, obtained from our developed package and SoundPLAN. In both figures, it can be observed that our developed package could produce highly reliable results in scenarios involving turbofan aircraft.

Specific to departure, the data points for CNT agreed very well with the benchmark, deviating over a range of





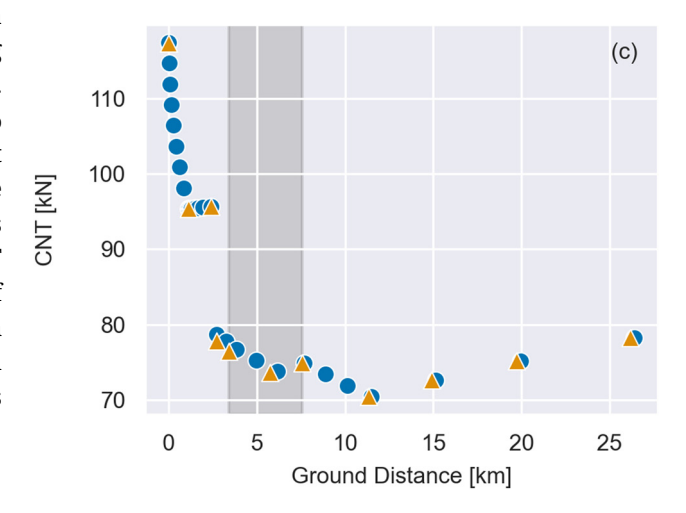


Figure 7: Departure flight profiles of the 737-8 MAX turbofan aircraft obtained from our developed package and SoundPLAN, showing (a) altitude, (b) CAS, and (c) CNT vs ground distance. Shaded region denotes the start of the third step to the end of the fourth step in the flight procedures (Table A4).

-0.1 to 1.1%. The data points for CAS deviated from the benchmark over a range of -5 to 0%. The lower limit was contributed by only one data point at the end of the transition step for thrust cutback. As discussed in Section

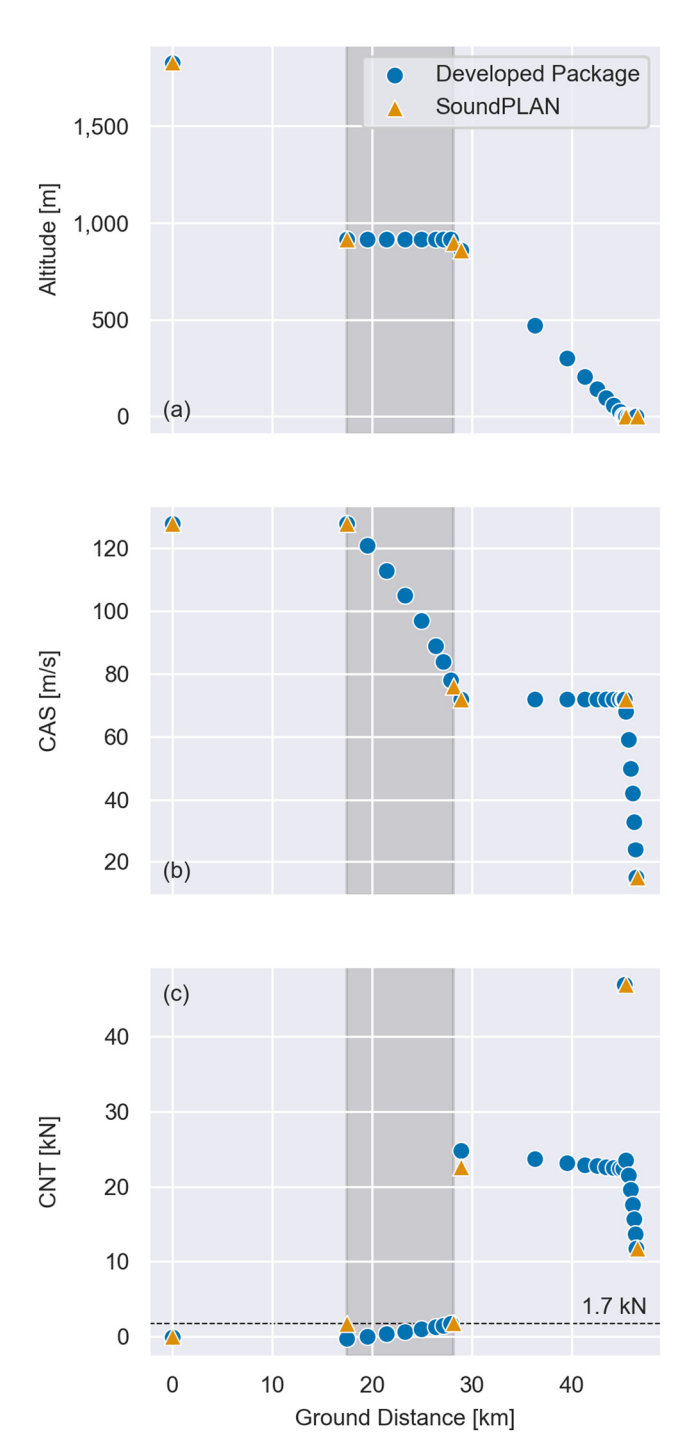


Figure 8: Arrival flight profiles of the 737-8 MAX turbofan aircraft obtained from our developed package and SoundPLAN, showing (a) altitude, (b) CAS, and (c) CNT vs ground distance. Shaded region denotes the start of the second step to the end of the fourth step in the flight procedures (Table A5).

3.2.1, the step was assumed to take place at a constant speed in our developed package. In contrast, SoundPLAN assumed acceleration, explaining why the aircraft arrived at 83 m/s earlier (Figure 7). Apart from this data point, the remaining data points for CAS matched exactly with the benchmark.

The data points for ground distance deviated from the benchmark over a range of 0-7.3%. Large discrepancies were observed between the third and fourth steps in the flight procedures (Table A4). As discussed in Section 3.2.1, the observation might be caused by the differences in how the iterative loops were coded compared to SoundPLAN. Similarly, large discrepancies were observed at the same data points for altitude. Overall, the data points deviated from the benchmark over a range of -0.7 to 15%. If the outliers were excluded, the data points for the respective parameters would deviate from the benchmark over a narrower range. For ground distance, it would be 0-1.6%. For altitude, it would be -0.7 to 7.5% in which the upper limit is now caused by the difference in assumptions made to compute the transition zone for thrust cutback (discussed in the preceding paragraph). If this data point was also excluded, the remaining data points would deviate from the benchmark over an even narrower range of -0.7 to 0%, suggesting strong agreement between them.

Specific to arrival, the data points for ground distance, altitude, and CAS agreed very well with the benchmark, deviating over a range of -1.1 to 0%, 0 to 1.8%, and 0 to 2.5%, respectively. The data points for CNT, excluding the data point at the start of the second step in the flight procedures (Table A5), deviated from the benchmark over a range of -4 to 9.6%. At the start of the second step, the noticeable discrepancy was caused by the difference in assumptions made to compute the CNT. In our developed package, the CNT was computed by substituting the idling engine coefficients and the prevailing CAS into equation (7). This assumption aligned well with the information given in the flight procedures [53] in which the aircraft should be flown at idling from the start of the first step to the end of the fourth step. Using this approach, the CNT at the moment when the aircraft completed the fourth step would be 1.7 kN. In contrast, SoundPLAN assumed constant CNT throughout the same steps, explaining why the benchmark value was at 1.7 kN as soon as the first step ended. As the basis for this assumption could not be fully understood, our developed package maintained consistency with the recommendations in the flight procedures.

The upper limit (9.6%) was contributed by the overestimation at the start of the final descent. In our developed package, the CNT (24.8 kN) was computed from equation (9) by having $\overline{F_n/\delta}$ as the subject with K=1.03 (Section 2.3.1.5), as specified in ECAC Doc 29 Vol 2. Investigations were conducted to uncover the exact values that Sound-PLAN had used to obtain the CNT of 22.6 kN. Similar to the findings in Section 3.2.1, it was challenging to troubleshoot

with a black box. Hence, assurance was established for the data point by ensuring that the correct values were retrieved and substituted into the correct equations.

3.3 Benchmarking the overall noise maps

Having established the reliability of the output produced by Module 1, the output of Module 2 was next benchmarked against SoundPLAN. Module 3 was used to generate the overall noise maps. Positional noise maps are not presented in this section because there were more than 20 frames involved in generating them (GIF files). Here, we present the noise maps in two sections to differentiate between turboprop (Section 3.3.1) and turbofan (Section 3.3.2) aircraft. For ease of interpretation, the noise maps ($L_{\rm Amax}$) are presented in metric units. The axes (equal aspect ratio) correspond to the ground distance in the x-and y-directions. As the nodal noise levels could not be easily extracted in SoundPLAN, we quantitatively conducted the benchmarking using the contour range.

3.3.1 Turboprop aircraft (C-130)

Figures 9 and 10 show the departure and arrival noise maps, respectively, obtained from our developed package and SoundPLAN. Both figures demonstrate the capability of our developed package to generate noise maps with accuracy comparable to the benchmark in scenarios involving turboprop aircraft. Given the strong agreement between the arrival noise maps, the following discussions will focus on departure.

Let us first direct our focus on the region of the noise map that is in front of the runway ($x \ge 0$ km). Between x = 39 km and x = 44 km, our developed package overestimated the noise levels below the flight path by one contour range. Instead of 50–60 dBA (benchmark), it was 60–70 dBA. In Figure 5, we observed that the data points for the respective parameters agreed well within the same range of ground distance. Hence, we deduced that the root cause of the overestimation should originate from the difference in certain assumptions made between SoundPLAN and Module 2, not Module 1. Owing to the black-box nature of SoundPLAN, identifying the difference in assumptions

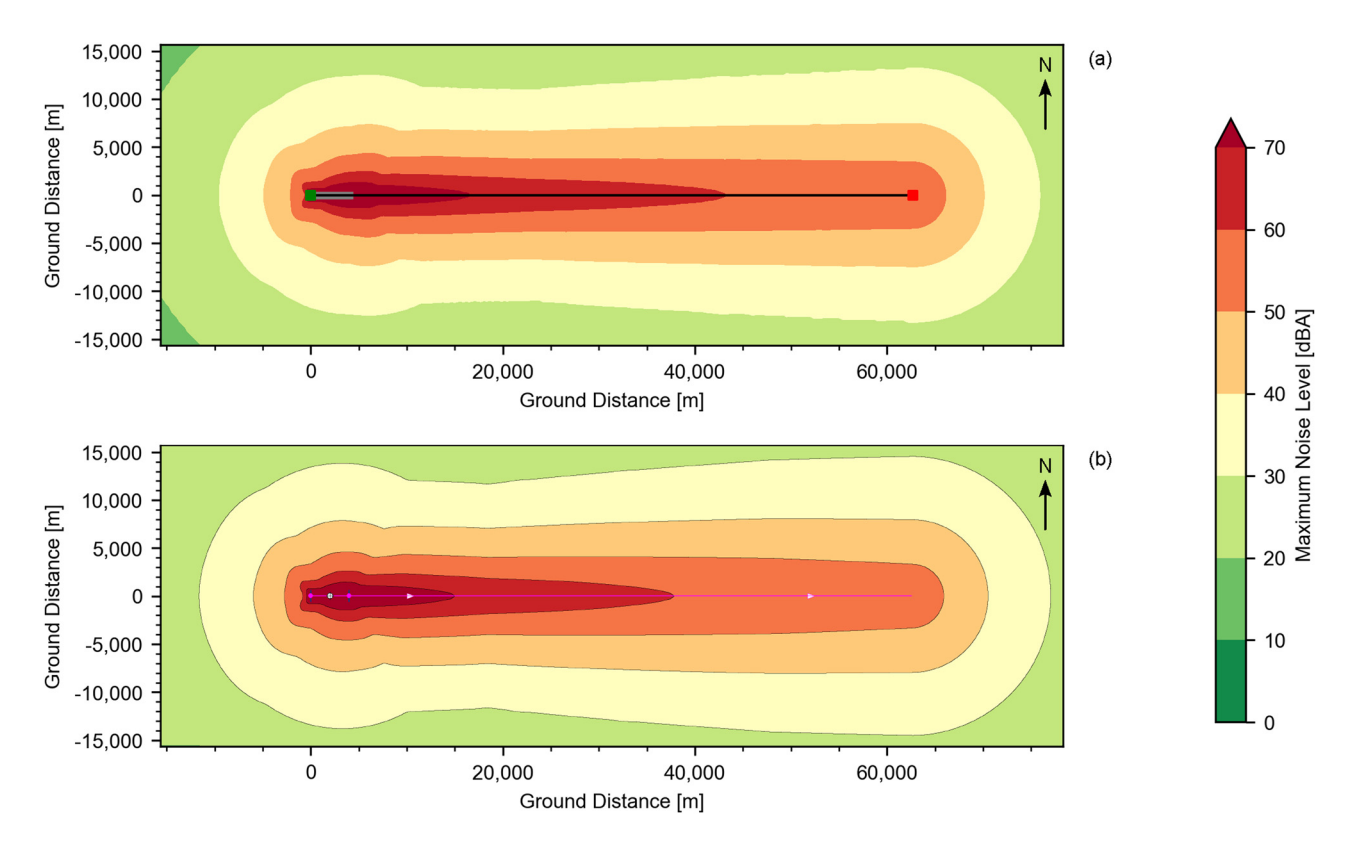


Figure 9: Departure noise maps of the C-130 turboprop aircraft: (a) our developed package and (b) SoundPLAN. In (a), green and red squares denote the start and end of the flight path (black solid line), respectively. The grey solid line denotes the runway.

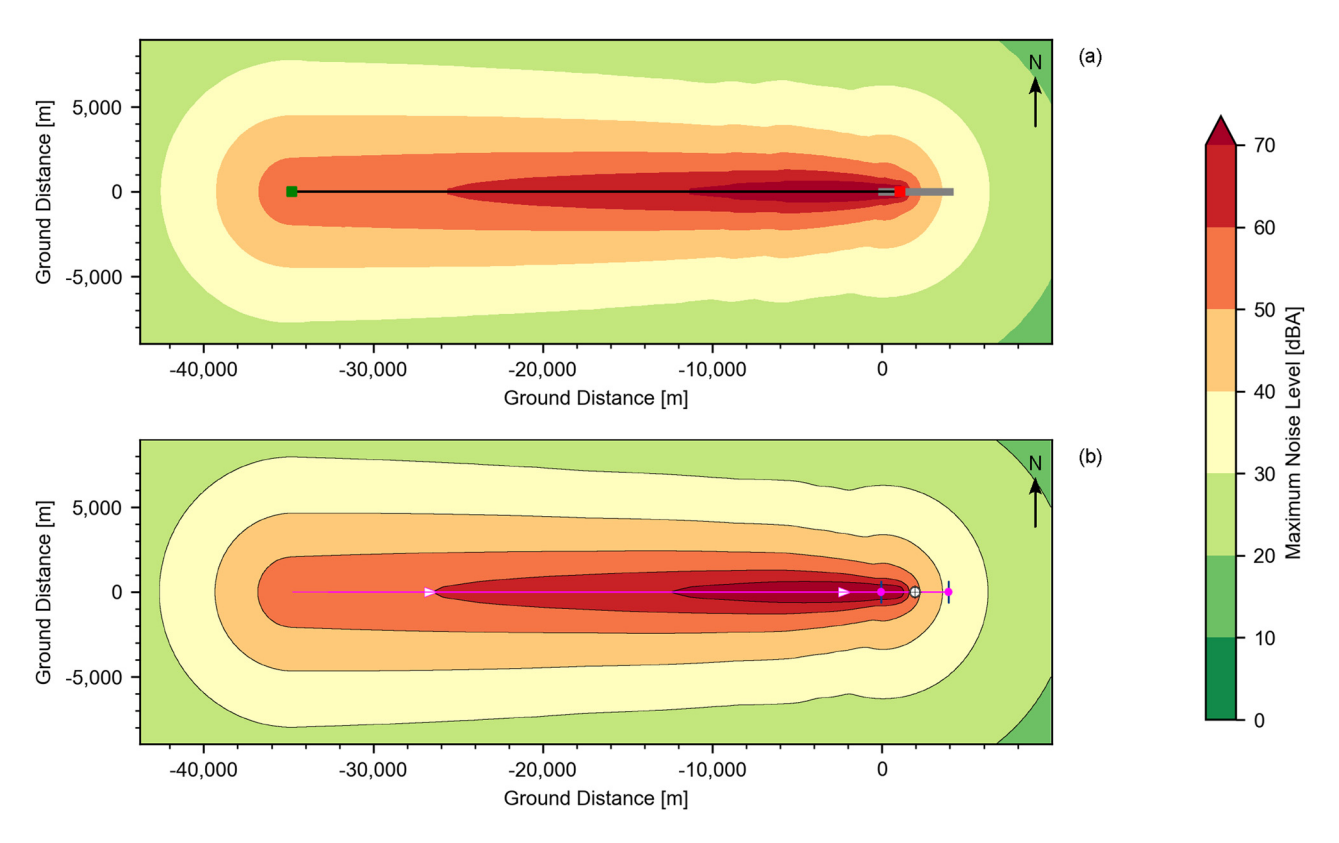


Figure 10: Arrival noise maps of the C-130 turboprop aircraft: (a) our developed package and (b) SoundPLAN. In (a), green and red squares denote the start and end of the flight path (black solid line), respectively. The grey solid line denotes the runway.

made had proved to be technically challenging. Nonetheless, we considered the achieved accuracy to be satisfactory because the modelling tool will be eventually used for noise impact assessments within Singapore. Therefore, we anticipate minimal demand from our target users to evaluate noise levels beyond a distance of 5 km from the aerodrome of interest.

Next, let us direct our focus on the region of the noise map that is behind the runway ($x \le 0$ km). Between x = -15km and x = -12 km, our developed package underestimated the noise levels between $y = \pm 11$ km and $y = \pm 15$ km. Instead of 20-30 dBA (benchmark), it was 10-20 dBA. In the underestimated zones, the noise levels were largely contributed by the takeoff ground roll. As the aircraft would only be farther away from the underestimated zones once it commenced takeoff, the noise levels there would naturally be lowered further. In reality, runways are typically surrounded by structures that contribute to minimising noise transmission beyond the aerodrome. Even in the absence of such structures, the ambient noise in the local environment should still exceed the aircraft noise (>30 dBA). In either scenario, considering the substantial distance and low noise levels, we anticipate minimal concern among our target users. Hence, we considered the achieved accuracy to be satisfactory.

3.3.2 Turbofan aircraft (737-8 MAX)

Figures 11 and 12 show the departure and arrival noise maps, respectively, obtained from our developed package and SoundPLAN. Again, both figures demonstrate the capability of our developed package to generate noise maps with accuracy comparable to the benchmark in scenarios involving turbofan aircraft. Given the strong agreement between the departure noise maps, the following discussions will focus on arrival.

Between x = -46 km and x = -39 km, our developed package overestimated the noise levels in the region below the flight path by one contour range (50–60 dBA instead of 40–50 dBA). We attributed the overestimation to the approach used in Module 2 to extrapolate the NPD values, as elaborated in Section 2.3.2. The NPD values listed in Table 1 can help provide further understanding. In the overestimated region, the direct distance between the aircraft and the receivers varied between 1,250 and 1,828 m. The CNT remained relatively constant, staying close to 0 kN because the aircraft was flown at idling. However, in Table 1, the lowest CNT is given as 13,345 kN, which is nowhere close to 0 kN. In such cases, Module 2 would execute the algorithms written to manage extrapolations and interpolations of the NPD values,

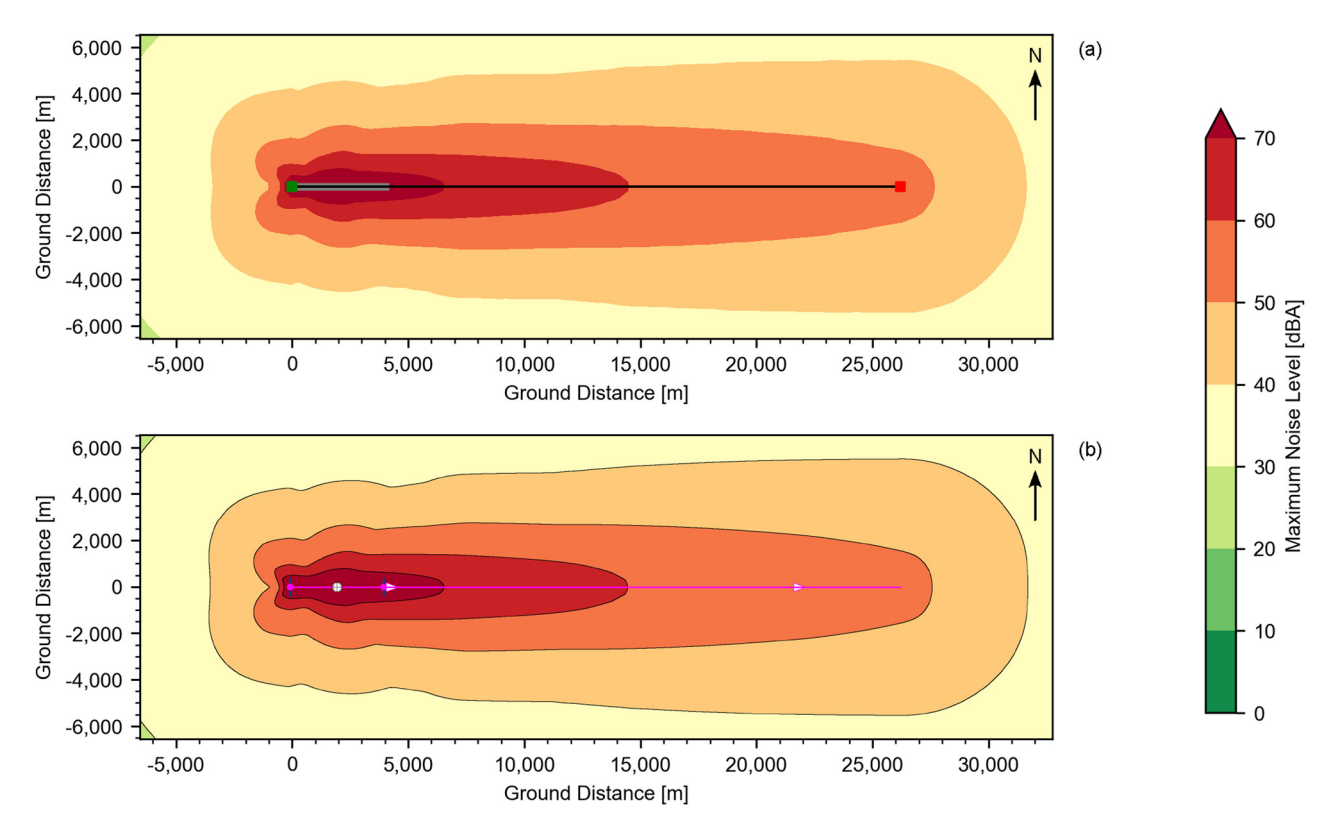


Figure 11: Departure noise maps of the 737-8 MAX turbofan aircraft: (a) our developed package and (b) SoundPLAN. In (a), green and red squares denote the start and end of the flight path (black solid line), respectively. The grey solid line denotes the runway.

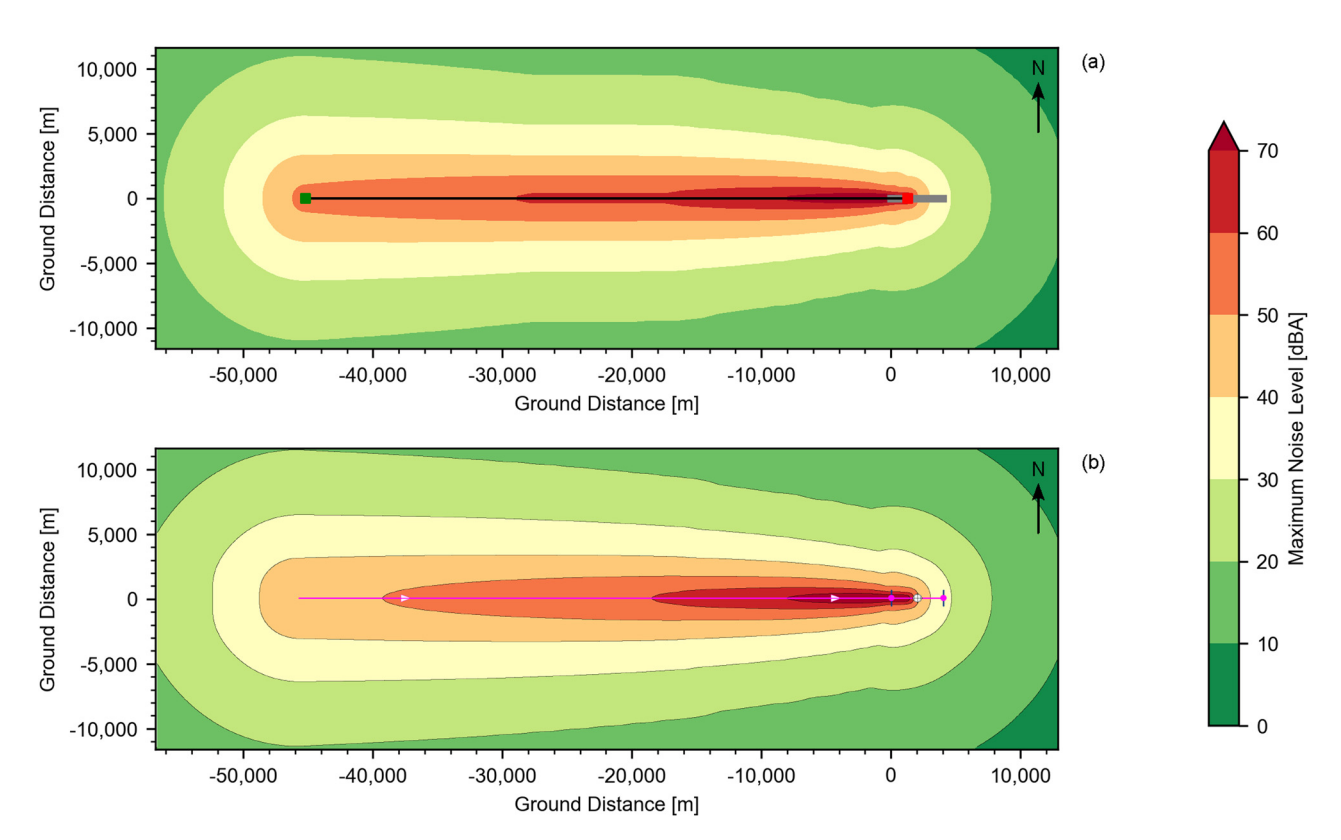


Figure 12: Arrival noise maps of the 737-8 MAX turbofan aircraft: (a) our developed package and (b) SoundPLAN. In (a), green and red squares denote the start and end of the flight path (black solid line), respectively. The grey solid line denotes the runway.

Table 1: Selected noise–power–distance (NPD) values (converted to metric units) of the 737-8 MAX turbofan aircraft [53]

		Direct distance (r	n)
CNT (kN)	610 (dBA)	1,219 (dBA)	1,920 (dBA)
13,345	65.9	57.1	50.7
17,793	65.9	57.1	50.6
22,241	66.1	57.2	50.7
26,689	66.5	57.6	51.0

Direct distance is measured from the aircraft to the receiver. Noise levels are expressed in $L_{\rm Amax}$.

as specified in ECAC Doc 29 Vol 2. By examining the noise levels in the first two rows, it becomes evident that the extrapolated noise levels would not decrease significantly. This lack of decrease is unexpected, particularly when the CNT is close to 0 kN. This explains why the noise levels were overestimated in our developed package, falling within the same contour range as those associated with the CNT listed in the first two rows. As mentioned earlier, our target users may have minimal demand to evaluate noise levels beyond a distance of 5 km from the aerodrome of interest. Hence, we considered the achieved accuracy to be satisfactory.

4 Discussion of the main limitations

In software development, limitations are necessary to shape the latest version so that design objectives can be achieved. These limitations can be associated with technical constraints, budgetary constraints, time constraints, and scope constraints. On the flip side, limitations can help prioritise enhancements for future work. As the software receives new updates through successive development cycles, it will gradually improve. In this section, the main limitations of our developed package are discussed, providing potential enhancements to consider for future work.

4.1 Supporting other noise metrics

For non-specialists, the $L_{\rm Amax}$ noise metric is typically preferred over other noise metrics because its concept is easy to fully comprehend. Although our developed package was designed for use by non-specialists, it is also important to support other noise metrics so that more options are available for consideration during noise impact assessments. As

mentioned in Section 2.2, quantifying aircraft noise is not limited to the $L_{\rm Amax}$ noise metric. Several other noise metrics exist for different purposes. Considering that our developed package is presently capable of creating only single-event scenarios, expressing the noise maps in terms of the sound exposure level ($L_{\rm AE}$) will naturally be one of the enhancements prioritised in the next developmental phase. This enhancement will largely impact Module 2 with added complexity arising from more mathematical expressions and situational requirements needed for computing the sound exposure level, as specified in ECAC Doc 29 Vol 2. Module 1 will also be updated to extract another set of NPD values from the embedded ANP database.

4.2 Supporting multiple-event scenarios

At times, our target users may wish to conduct noise impact assessments for a multiple-event scenario, which involves more than one departure or arrival. In contrast, a singleevent scenario allows only one departure or arrival to be considered. For example, a multiple-event scenario can provide a more comprehensive description of the flight operations at an international airport. This enhancement will mainly impact Module 1. In practice, each aircraft may deviate from the intended flight path to some extent, especially during the initial climb. Collectively, the deviations contribute to the lateral spreading of ground tracks perpendicular to the intended ground track. ECAC Doc 29 Vol 2 specifies that the deviations were found to follow a Gaussian distribution with the main flight at the centre. Hence, Module 1 will need a new set of algorithms to account for ground track spreading, apart from extracting more aircraft data from the embedded database.

4.3 Combining departure and arrival scenarios

If multiple-event scenarios can eventually be supported, our target users may be interested in studying the combined effects of multiple departing and arriving flights within the same scenario. Currently, our developed package can only consider departing and arriving flights as independent scenarios. Again, Module 1 will be largely impacted by this enhancement. In addition to what was discussed in Section 4.2, Module 1 will need another set of algorithms to correctly merge both departure and arrival flight profiles (spatial information and values of the performance parameters).

4.4 Displaying safety noise limits

When noise maps are generated, our target users may not always be certain of the safety noise limits, which determine whether the neighbourhood may be facing potential noise issues. These noise limits can vary depending on the regulations that local authorities take reference from. Therefore, displaying the noise limits with respect to the local regulations in the GUI is believed to benefit our target users. However, it is also important to note that this enhancement will only be possible if the corresponding noise metrics are supported in the first place. This enhancement will particularly impact Module 3, which is responsible for handling the visual aspects of the noise maps.

4.5 Calculating facade noise level

If our target users aim to evaluate the noise impact within an existing neighbourhood, our developed package currently lacks the ability to account for the physical existence of buildings. In densely populated urban areas, having existing buildings in the study area is nearly unavoidable. Thus, incorporating the representation of buildings into our developed package is a crucial priority. Furthermore, the capability to calculate noise levels specifically on building facades becomes essential for subsequent studies pertaining to noise mitigation within residential spaces. This enhancement will impact Modules 2 and 3. In particular, Module 2 will need a new set of algorithms responsible for importing threedimensional building models, generating facade nodes, and calculating nodal noise levels while accounting for the relevant sound propagation physics.

5 Conclusion

In conclusion, this article has presented the development and benchmarking of a package designed to easily generate aircraft noise maps via simplified procedures and a reduced amount of input data, with acceptable accuracy in the results. These benefits distinguish our developed package from commercial software. However, we must stress that the results produced by our developed package are intended primarily for quick evaluation and should be regarded as approximate. Ultimately, it is advisable to validate the results through field measurement data and benchmarking with commercial software tailored for comprehensive noise calculations. Our developed package was eventually integrated

into an in-house-developed unified urban environmental modelling tool that aims to help urban planners design more liveable and sustainable residential towns in an intuitive and quick manner. By regularly seeking feedback from our target users through trial runs, future work will help address the current limitations and improve the GUI and functionality of our developed package. When ready, we can consider the unified urban environmental modelling tool for external use.

Acknowledgements: We would like to thank Mr. Senthil Kumar Selvara and Ms. Fiona Liausvia from the Institute of High Performance Computing, A*STAR, for working closely with us to design and develop the GUI specific to the aircraft noise mapping feature.

Funding information: This research is supported by the National Research Foundation, Singapore.

Author contributions: L.Y.L.A.: conceptualisation, methodology, software, benchmarking, formal analysis, data curation, writing - original draft, visualisation. F.C.: conceptualisation, methodology, resources, writing – review & editing, supervision, project administration, funding acquisition. H.J.P.: resources, writing – review & editing, supervision, project administration, funding acquisition.

Conflict of interest: We declare no known competing financial interests or personal relationships that could have appeared to influence the research reported in this article.

Data availability statement: The data generated in this research are not made available publicly.

References

- Asdrubali F, D'Alessandro F. Innovative approaches for noise management in smart cities: A review. Current Pollution Reports. 2018;4(2):143-53.
- [2] Liu Y, Ma X, Shu L, Yang Q, Zhang Y, Huo Z, et al. Internet of Things for noise mapping in smart cities: State of the art and future directions. IEEE Network. 2020;34(4):112-8.
- Alias F, Alsina-Pagés RM. Review of wireless acoustic sensor networks for environmental noise monitoring in smart cities. J Sensors. 2019;2019:1-13.
- Licitra G, Artuso F, Bernardini M, Moro A, Fidecaro F, Fredianelli L. [4] Acoustic beamforming algorithms and their applications in environmental noise. Current Pollution Reports. 2023;9(3):486-509.
- Shah SK, Tariq Z, Lee J, Lee Y. Real-time machine learning for air quality and environmental noise detection. In: Proceedings of the 2020 IEEE International Conference on Big Data (Big Data). Atlanta, GA, USA: IEEE; 2020. p. 3506-15.

- [6] Renaud J, Karam R, Salomon M, Couturier R. Deep learning and gradient boosting for urban environmental noise monitoring in smart cities. Expert Syst Appl. 2023;218:119568.
- [7] Nourani V, Gökçekuş H, Umar IK. Artificial intelligence based ensemble model for prediction of vehicular traffic noise. Environ Res. 2020;180:108852.
- Fredianelli L, Carpita S, Bernardini M, Del Pizzo LG, Brocchi F, Bianco F, et al. Traffic flow detection using camera images and machine learning methods in its for noise map and action plan optimisation. Sensors. 2022;22(5):1929.
- López JM, Alonso J, Asensio C, Pavón I, Gascó L, De Arcas G. A digital signal processor based acoustic sensor for outdoor noise monitoring in smart cities. Sensors. 2020;20(3):605.
- [10] Ballesteros JA, Sarradj E, Fernández MD, Geyer T, Ballesteros MJ. Noise source identification with beamforming in the pass-by of a car. Appl Acoustics. 2015;93:106-19.
- [11] Pallas MA, Bérengier M, Chatagnon R, Czuka M, Conter M, Muirhead M. Towards a model for electric vehicle noise emission in the European prediction method CNOSSOS-EU. Appl Acoustics. 2016;113:89-101.
- [12] Licitra G, Bernardini M, Moreno R, Bianco F, Fredianelli L. CNOSSOS-EU coefficients for electric vehicle noise emission. Appl Acoustics. 2023;211:109511.
- [13] Steinbach L, Altinsoy ME. Prediction of annoyance evaluations of electric vehicle noise by using artificial neural networks. Appl Acoustics. 2019;145:149-58.
- [14] Ascari E, Cerchiai M, Fredianelli L, Melluso D, Rampino F, Licitra G. Decision trees and labeling of low noise pavements as support for noise action plans. Environ Pollution. 2023;337:122487.
- [15] Ascari E, Cerchiai M, Fredianelli L, Licitra G. Statistical pass-by for unattended road traffic noise measurement in an urban environment. Sensors. 2022;22(22):8767.
- [16] Smite D, Moe NB, Hildrum J, Gonzalez-Huerta J, Mendez D. Workfrom-home is here to stay: Call for flexibility in post-pandemic work policies. J Syst Softw. 2023;195:111552.
- [17] George TJ, Atwater LE, Maneethai D, Madera JM. Supporting the productivity and wellbeing of remote workers: Lessons from COVID-19. Organisational Dynam. 2022;51(2):100869.
- [18] Wothge J, Belke C, Möhler U, Guski R, Schreckenberg D. The combined effects of aircraft and road traffic noise and aircraft and railway noise on noise annoyance-An analysis in the context of the joint research initiative NORAH. Int J Environ Res Public Health. 2017;14(8):871.
- [19] Schäffer B, Brink M, Schlatter F, Vienneau D, Wunderli JM. Residential green is associated with reduced annoyance to road traffic and railway noise but increased annoyance to aircraft noise exposure. Environ Int. 2020;143:105885.
- [20] WHO. Environmental Noise Guidelines for the European Region. Copenhagen, Denmark: World Health Organisation; 2019.
- Beutel ME, Jünger C, Klein EM, Wild P, Lackner K, Blettner M, et al. Noise annoyance is associated with depression and anxiety in the general population-The contribution of aircraft noise. PLoS One. 2016;11(5):e0155357.
- [22] Ang LYL, Cui F. Remote work: Aircraft noise implications, prediction, and management in the built environment. Appl Acoustics. 2022;198:108978.
- [23] Sparrow V, Gjestland T, Guski R, Richard, Basner M, Hansell A, et al. State of the science 2019: Aviation noise impacts. In: ICAO Environmental Report 2019. Montreal, Canada: International Civil Aviation Organisation; 2019. p. 44-61.

- [24] Babisch W. Updated exposure-response relationship between road traffic noise and coronary heart diseases: A meta-analysis. Noise Health. 2014;16(68):1-9.
- [25] Cohen JP, Coughlin CC. Spatial hedonic models of airport noise, proximity, and housing prices. J Regional Sci. 2008;48(5):859-78.
- [26] O'Byrne PH, Nelson JP, Seneca JJ. Housing values, census estimates, disequilibrium, and the environmental cost of airport noise: A case study of Atlanta, I Environ Econ Manag, 1985;12(2):169-78.
- Mahmoud NSA, Jung C, Al Qassimi N. Evaluating the aircraft noise level and acoustic performance of the buildings in the vicinity of Dubai International Airport. Ain Shams Eng J. 2023;14(8):102032.
- Bueno AM, de Paula Xavier AA, Broday EE. Evaluating the connection between thermal comfort and productivity in buildings: A systematic literature review. Buildings. 2021;11(6):244.
- [29] Postorino MN, Mantecchini L. A systematic approach to assess the effectiveness of airport noise mitigation strategies. J Air Transport Manag. 2016;50:71-82.
- [30] Licitra G, Gagliardi P, Fredianelli L, Simonetti D. Noise mitigation action plan of Pisa civil and military airport and its effects on people exposure. Appl Acoustics. 2014;84:25-36.
- Behere A, Mavris DN. Optimisation of takeoff departure procedures for airport noise mitigation. Trans Res Record J Transport Res Board. 2021;2675(9):81-92.
- [32] Gagliardi P, Fredianelli L, Simonetti D, Licitra G. ADS-B system as a useful tool for testing and redrawing noise management strategies at Pisa Airport. Acta Acustica united with Acustica. 2017;103(4):543-51.
- Arafa MH, Osman TA, Abdel-Latif IA. Noise assessment and miti-[33] gation schemes for Hurghada Airport. Appl Acoustics. 2007;68(11-12):1373-85.
- [34] Yang YL. Comparison of public perception and risk management decisions of aircraft noise near Taoyuan and Kaohsiung International Airports. J Air Transport Manag. 2020;85:101797.
- [35] Kwak KM, Ju YS, Kwon YJ, Chung YK, Kim BK, Kim H, et al. The effect of aircraft noise on sleep disturbance among the residents near a civilian airport: A cross-sectional study. Annal Occupat Environ Med. 2016;28(1):38.
- [36] Choy J. Mitigating the impact of Tengah Airbase on residences [Bachelor's Thesis]. Republic of Singapore: National University of Singapore: 2020. https://scholarbank.nus.edu.sg/handle/10635/220285.
- [37] Lee HP, Kumar S, Garg S, Lim KM. Characteristics of aircraft flypast noise around Singapore Changi International Airport. Appl Acoustics. 2022;185:108418.
- [38] Di G, Liu X, Shi X, Li Z, Lin Q. Investigation of the relationship between aircraft noise and community annoyance in China. Noise Health. 2012;14(57):52.
- [39] Basner M, Barnett I, Carlin M, Choi GH, Czech JJ, Ecker AJ, et al. Effects of aircraft noise on sleep: Federal Aviation Administration National Sleep Study protocol. Int J Environ Res Public Health. 2023;20(21):7024.
- [40] Heinonen-Guzejev M, Vuorinen HS, Kaprio J, Heikkilä K, Mussalo-Rauhamaa H, Koskenvuo M. Self-report of transportation noise exposure, annoyance and noise sensitivity in relation to noise map information. J Sound Vibration. 2000;234(2):191-206.
- [41] King EA, Rice HJ. The development of a practical framework for strategic noise mapping. Appl Acoustics. 2009;70(8):1116-27.
- [42] Wunderli JM, Zellmann C, Köpfli M, Habermacher M. sonAIR-A GISintegrated spectral aircraft noise simulation tool for single flight prediction and noise mapping. Acta Acustica united with Acustica. 2018;104(3):440-51.

- [43] Jäger D, Zellmann C, Schlatter F, Wunderli JM. Validation of the sonAIR aircraft noise simulation model. Noise Mapping. 2021;8(1):95–107.
- [44] Meister J, Schalcher S, Wunderli JM, Jäger D, Zellmann C, Schäffer B. Comparison of the aircraft noise calculation programs sonAIR, FLULA2, and AEDT with noise measurements of single flights. Aerospace. 2021;8(12):388.
- [45] Riboldi CED, Trainelli L, Mariani L, Rolando A, Salucci F. Predicting the effect of electric and hybrid-electric aviation on acoustic pollution. Noise Mapping. 2020;7(1):35–56.
- [46] ECAC. ECAC Doc 29 Vol 1: Report on Standard Method of Computing Noise Contours Around Civil Airports–Applications Guide. 4th ed. Neuilly-sur-Seine, France: European Civil Aviation Conference: 2016.
- [47] ECAC. ECAC Doc 29 Vol 2: Report on Standard Method of Computing Noise Contours Around Civil Airports–Technical Guide. 4th ed. Neuilly-sur-Seine, France: European Civil Aviation Conference; 2016.
- [48] ECAC. ECAC Doc 29 Vol 3 Part 1: Report on Standard Method of Computing Noise Contours Around Civil Airports-Reference Cases and Verification Framework. 4th ed. Neuilly-sur-Seine. 4th ed. Neuilly-sur-Seine, France: European Civil Aviation Conference; 2016.

- [49] EU. Directive 2002/49/EC: Assessment and Management of Environmental Noise. Brussels, Belgium: European Union; 2002.
- [50] Yang C, Mott JH. Developing a cost-effective assessment method for noise impacts at non-towered airports: A case study at Purdue University. Transport Res Record J Transport Res Board. 2022;2676(12):786–97.
- [51] Nakazawa T, Sugawara M, Shinohara N, Yamada I. Difference in airport noise calculation procedures between AERC model and ECAC Doc 29. In: Proceedings of the 46th International Congress and Exposition on Noise (INTER-NOISE 2017). Hong Kong, China: Institute of Noise; 2017. p. 2640.
- [52] Liu V. Researchers who created urban planning simulation model for Tengah wins President's Technology Award. The Straits Times. 2019. Accessed Jul 1, 2023. https://www.straitstimes.com/ singapore/researchers-who-created-urban-planning-simulationmodel-for-tengah-wins-presidents.
- [53] EUROCONTROL. The Aircraft Noise and Performance (ANP) Database: An international data resource for aircraft noise modellers. EUROCONTROL. 2020. Accessed Jul 1, 2023. https://www.aircraftnoisemodel.org/.
- [54] ISO. ISO 2533: Standard Atmosphere. Geneva, Switzerland: International Organisation for Standardisation; 1975.

Appendix

A Default values of the essential parameters

This section provides supplementary information on the default values of the essential parameters given to the user in the GUI (Table A1). Unlike commercial software, our developed package can easily generate reliable noise maps as long as the user selects the aircraft model and the

Table A1: Default values of the essential parameters given to the user in the GUI

Module	Parameter	Value	Unit
1	Ambient air pressure	101.325	kPa
	Ambient air temperature	15	° C
	Headwind	4.12	m/s
	Runway elevation	0	m
	Runway gradient	0	_
	Runway length	4,000	m
	Runway heading	90	0
2	Plane type	Automatic	_
	Plane altitude	0	m
	Grid size	304.8	m
	Lateral coverage factor	0.25	_
3	Contour range	0-70	dBA
	Contour interval	5	dBA
	Aspect ratio	Equal axes	_
	Display runway	Yes	_
	Display ground track	Yes	_

flight type. Although imperial units are preferred in the aviation sector, the GUI was designed with ease of use in mind, using metric units for all inputs. Units are converted in the back-end.

B Default flight procedures

For every aircraft, the manufacturer publishes the default flight procedures that can be used as a reference to how the aircraft is being operated during departure or arrival. This section provides the supplementary information on the default flight procedures (departure and arrival) [53] for the C-130 aircraft (Tables A2 and A3) and 737-8 MAX aircraft (Tables A4 and A5).

Table A2: Default flight procedures for the C-130 aircraft during departure

No.	Step type	Thrust rating	Final altitude (ft)	ROC (ft/min)	Final CAS (kt)
1	Ground roll	Max takeoff			
2	Initial climb	Max takeoff	1,000		
3	Acceleration	Max takeoff		1,423	142
Transitio	n step for thrust cutback				
4	Acceleration	Max climb		1,068	162
5	Constant speed	Max climb	3,000		
6	Acceleration	Max climb		1,000	200
7	Constant speed	Max climb		5,500	
8	Constant speed	Max climb		7,500	
9	Constant speed	Max climb		10,000	

ROC and CAS denote the rate of climb and the calibrated airspeed, respectively.

Table A3: Default flight procedures for the C-130 aircraft during arrival

No.	Step type	Initial altitude (ft)	Initial CAS (kt)	Descent angle (deg)	Distance (ft)	Initial thrust (%)
1	Descent	6,000	200	3		
2	Descent	3,000	166	3		
3	Descent	1,500	146	3		
4	Final descent	1,000	136	3		
5	Touchdown				341	
6	Ground roll		129		3,070	40
7	Taxiing		30			10

CAS denotes the calibrated airspeed.

Table A4: Default flight procedures for the 737-8 MAX aircraft during departure

No.	Step type	Thrust rating	Final altitude (ft)	ROC (ft/min)	Final CAS (kt)
1	Ground roll	Max takeoff			
2	Initial climb	Max takeoff	1,000		
Transitio	n step for thrust cutback				
3	Acceleration	Max climb		1,336	174
4	Acceleration	Max climb		1,799	205
5	Constant speed	Max climb	3,000		
6	Acceleration	Max climb		1,681	250
7	Constant speed	Max climb		5,500	
8	Constant speed	Max climb		7,500	
9	Constant speed	Max climb		10,000	

ROC and CAS denote the rate of climb and the calibrated airspeed, respectively.

Table A5: Default flight procedures for the 737-8 MAX aircraft during arrival

No.	Step type	Initial altitude (ft)	Initial CAS (kt)	Descent angle (deg)	Distance (ft)	Initial thrust (%)
1	Descent	6,000	250	3		
2	Level	3,000	250		24,557	
3	Level	3,000	189		4,678	
4	Level	3,000	174		4,907	
5	Descent	3,000	152	3		
6	Final descent	2,817	139	3		
7	Touchdown				394	
8	Ground roll		139		3,838	40
9	Taxiing		30			10

CAS denotes the calibrated airspeed.